AD-A128 142 ANALYSIS OF A DIFFUSION WAVE FLOW ROUTING MODEL WITH APPLICATION TO FLOW IN WATERS(U) COLD REGIONS RESEARCH AND ENGINEERING LAB HANOVER NH M G FERRICK ET AL. 1/1

UNCLASSIFIED MAR 83 CRREL-83-7 F/G 20/4 NL

END
DATE FILMED
6-83
DTIC

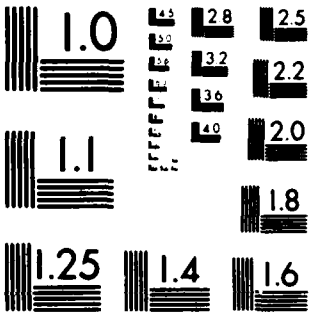

CRREL
REPORT 83-7

US Army Corps
of Engineers
Cold Regions Research &
Engineering Laboratory

Analysis of a diffusion wave flow routing model with application to flow in tailwaters

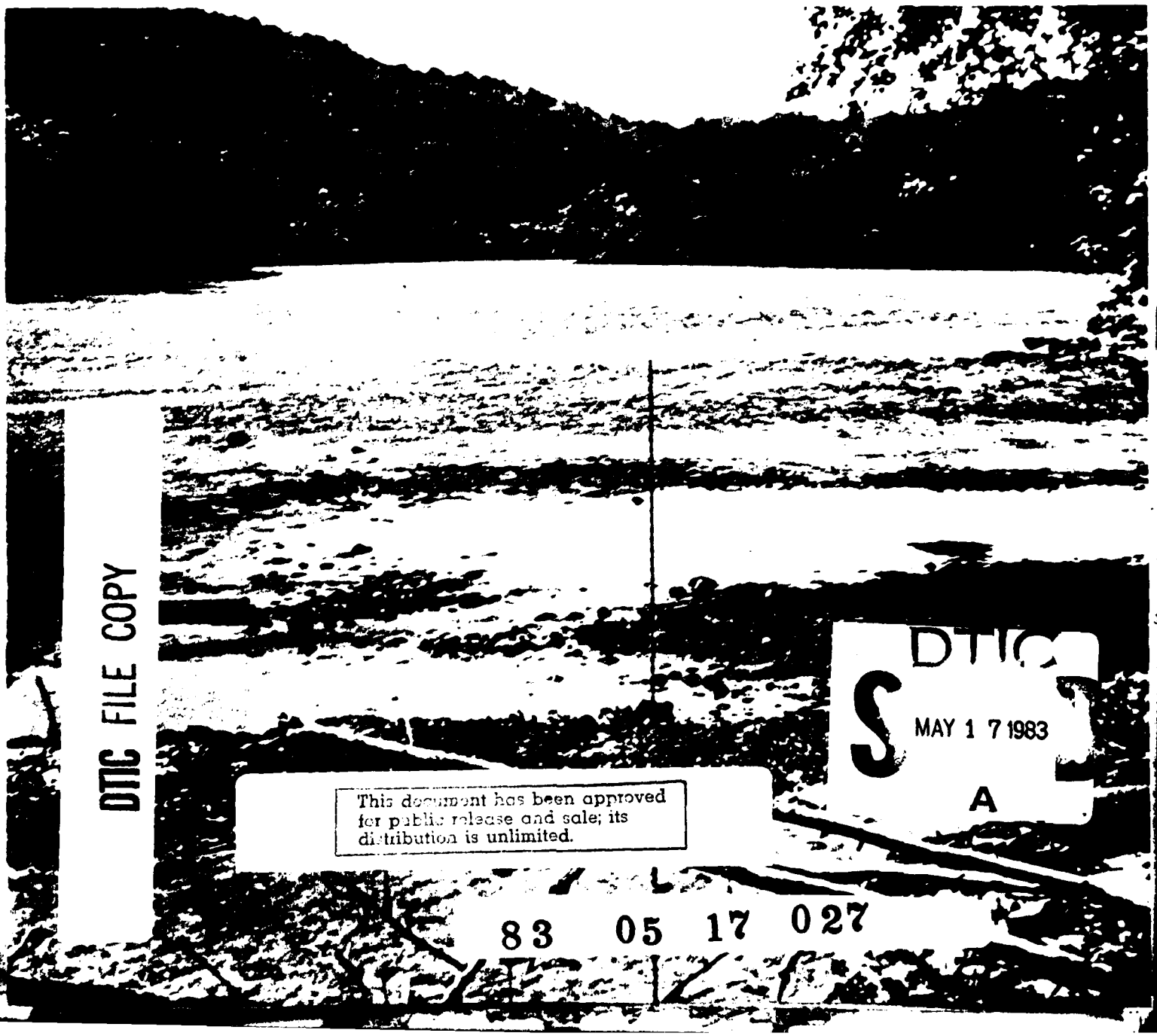

For conversion of SI metric units to U.S./British customary units of measurement consult ASTM Standard E380, Metric Practice Guide, *published by the American Society for Testing and Materials, 1916 Race St., Philadelphia, Pa. 19103.*

Cover: Front of a wave propagating downstream at Clinch River mile 78.7 during field tests, July 1980. The wave was produced by an abrupt flow release at Norris Dam, approximately 1 mile upstream. (Photograph by M. Ferrick.)

CRREL Report 83-7

March 1983

Analysis of a diffusion wave flow routing model with application to flow in tailwaters

M.G. Ferrick, J. Bilmes and S.E. Long

Prepared for
OFFICE OF THE CHIEF OF ENGINEERS

Unclassified

SECURITY CLASSIFICATION OF THIS PAGE (When Data Entered)

REPORT DOCUMENTATION PAGE		READ INSTRUCTIONS BEFORE COMPLETING FORM
1. REPORT NUMBER CRREL Report 83-7	2. GOVT ACCESSION NO. AD-A128 142	3. RECIPIENT'S CATALOG NUMBER
4. TITLE (and Subtitle) ANALYSIS OF A DIFFUSION WAVE FLOW ROUTING MODEL WITH APPLICATION TO FLOW IN TAILWATERS		5. TYPE OF REPORT & PERIOD COVERED 6. PERFORMING ORG. REPORT NUMBER
7. AUTHOR(s) M.G. Ferrick, J. Bilmes and S.E. Long		8. CONTRACT OR GRANT NUMBER(s)
9. PERFORMING ORGANIZATION NAME AND ADDRESS U.S. Army Cold Regions Research and Engineering Laboratory Hanover, New Hampshire 03755		10. PROGRAM ELEMENT, PROJECT, TASK AREA & WORK UNIT NUMBERS DA Project 4A161102AT24 Area B, Work Unit 003
11. CONTROLLING OFFICE NAME AND ADDRESS Office of the Chief of Engineers Washington, D.C. 20314		12. REPORT DATE March 1983 13. NUMBER OF PAGES 41
14. MONITORING AGENCY NAME & ADDRESS(if different from Controlling Office)		15. SECURITY CLASS. (of this report) Unclassified 15a. DECLASSIFICATION/DOWNGRADING SCHEDULE

16. DISTRIBUTION STATEMENT (of this Report)

Approved for public release; distribution unlimited.

17. DISTRIBUTION STATEMENT (of the abstract entered in Block 20, if different from Report)

18. SUPPLEMENTARY NOTES

19. KEY WORDS (Continue on reverse side if necessary and identify by block number)

Dams	Peak power
Flow routing	Rivers
Hydrology	Water flow
Mathematical analysis	Waves
Numerical methods	

20. ABSTRACT (Continue on reverse side if necessary and identify by block number)

Peak power generation with hydropower creates tailwater flow conditions characterized by high and low flows with abrupt transitions between these states. Flows occurring in tailwaters typically form sharp-fronted, large-amplitude waves of relatively short period. An understanding of the mechanics of downstream propagation of these waves is important both for direct application in studies of the tailwater and because of the similarity of these waves to those following a dam break. An analysis of the dynamic equations of open channel flow is used to quantify the relative importance of flow wave convection, diffusion and dispersion in rivers. The relative importance of each process is related to the relative magnitude of terms in the dynamic equations, providing a physical basis for model formulation.

DD FORM 1 JAN 73 1473 EDITION OF 1 NOV 65 IS OBSOLETE

Unclassified

SECURITY CLASSIFICATION OF THIS PAGE (When Data Entered)

20. Abstract (cont'd).

A one-dimensional diffusion wave flow routing model, modified for tailwaters, simulates the important physical processes affecting the flow and is straightforward to apply. The model is based upon a numerical solution of the kinematic wave equation. The "modified equation," Hirt, and von Neumann analyses are used to gain insight into the stability and dissipative and dispersive behavior of the numerical solution, and results of these analyses are compared. A set of linear routings is used to demonstrate the dissipative and dispersive behavior predicted by the analyses and to verify the accuracy of an expression that quantifies the numerical diffusion of the model. The analyses provide a basis for selection of numerical parameters for model applications. The capability and accuracy of the model are enhanced when physical wave diffusion is balanced by numerical diffusion in the model. Maintaining the diffusion balance requires that the time derivative weighting parameter θ be variable and in some instances negative. Though some amount of phase error is introduced, negative θ values have no adverse effect upon model stability. Field studies were conducted to demonstrate the benefits of careful model development and analysis, and to verify the diffusion wave model for rapidly varying tailwater flow. The bed slope and roughness characteristics of the field study reaches (below Apalachia and Norris Dams) differ greatly, spanning those of a large number of rivers of practical interest. The accurate simulation of flow in both of these tailwaters attests to the soundness of both the physical basis of the model and the numerical solution technique. The field studies confirm, for the extreme case of rapidly varying flow in a mildly sloped river, that inertia has a negligible effect upon unsteady flow waves at low Froude numbers. Additionally, these studies verify that diffusion of short-period waves in rivers is generally significant.

PREFACE

This report was prepared by M.G. Ferrick, Hydrologist, of the Snow and Ice Branch, Research Division, U.S. Army Cold Regions Research and Engineering Laboratory, J. Bilmes, a graduate student in the Department of Civil Engineering, University of Michigan, and S.E. Long, Civil Engineering Associate, of Water Systems Development Branch, Tennessee Valley Authority. Funding for this research was provided by DA Project 4A161102AT24, *Research in Snow, Ice and Frozen Ground,* Scientific Area B, *Cold Regions Environmental Interactions,* Work Unit 003, *Snow and Ice Geophysical Processes.*

The author thanks Dr. George Ashton and Dr. Charles Daly for technically reviewing this report and numerous individuals in the TVA Division of Water Resources for their help with the field investigations.

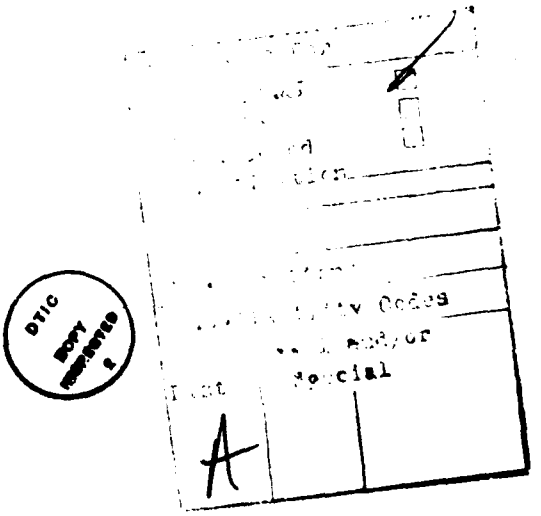

CONTENTS

ILLUSTRATIONS

NOMENCLATURE

a	damping exponent, modified equation analysis
A	cross-sectional area of the channel
b	phase exponent, modified equation analysis
B	channel width
c	wave celerity
$\bar{c}$	average wave celerity in a reach
C	Chezy conveyance coefficient
C_m	constant, Manning's equation
C_r	Courant number
D	diffusion coefficient
D^*	dimensionless diffusion coefficient
E	dispersion coefficient
E_H	dispersion coefficient, Hirt analysis
E^*	dimensionless dispersion coefficient
F	Froude number
g	acceleration due to gravity
j	spatial index
k	wave number
m	time index
n	Manning's roughness coefficient
$O( )$	the order of
q	discharge per unit width
q_i	local inflow per unit length of channel
Q	discharge
Q_k	amplitude of the discharge component of wave number, k
Q_0	discharge at previous time step
Q^*	dimensionless discharge
$\dot{Q}$	derivative of discharge with respect to time
R	channel hydraulic radius
r_k	complex amplification factor of the k-th Fourier component
S_f	slope of the energy grade line
S_0	slope of the channel bottom
t	time
t^*	dimensionless time
V	velocity
x	distance
x^*	dimensionless distance
y	flow depth
y_0	flow depth at previous time step
$\Delta x, \Delta t$	finite distance and time increments
α	grouping of parameters, diffusion wave model
β	grouping of parameters, diffusion wave model
γ	$k\Delta x$
θ	balanced diffusion parameter, diffusion wave model
μ	coefficients of terms in the modified equation
Φ_c	phase angle of continuum solution
Φ_N	phase angle of numerical solution
Φ_r	ratio of numerical and continuum phase angles
$< >$	average over time, Δt

ANALYSIS OF A DIFFUSION WAVE FLOW ROUTING MODEL WITH APPLICATION TO FLOW IN TAILWATERS

M.G. Ferrick, J. Bilmes and S.E. Long

INTRODUCTION

Current concerns regarding energy resources have sparked renewed interest in hydroelectric power generation. Hydropower is especially valuable as it is well suited to meeting the peak power demands of a utility. Peak power generation with hydropower yields flow regimes in tailwater streams that are characteristically high or low with sharp transitions between these states. Large flow and stage changes can occur in a tailwater in a period of several minutes. The duration of a zero flow release can vary widely with power demand and water availability.

Lengthy periods of zero flow affect the ability of a tailwater to maintain a healthy aquatic ecosystem. Water temperature and quality in tailwaters are modified from those occurring naturally in the stream, and sharp stage transitions can disrupt a stable river ice cover in northern rivers. Accurate knowledge of the flow regime is an important component of an assessment of the potential effects of peak power generation upon alternative uses of the stream. In addition, an understanding of downstream-propagating sharp-fronted, large-amplitude flow waves of relatively short period is important because of their similarity to dam break waves.

Numerical models can be used to investigate the flow regime of a tailwater. The development of such a numerical model has two basic parts that we will address in this report. The first is the construction of the mathematical statement of the physical processes of primary interest. The second basic part is the development and analysis of the numerical solution technique. It is this second component of model development that often does not receive adequate attention. As a result, the behavior of a model is not well understood, and guidance is unavailable concerning parameter selection to achieve optimal accuracy for a given application and interpretation of model output.

We performed an analysis of the dynamic open channel flow equations to obtain insight regarding the physical processes of importance in tailwater flow. The relative magnitudes of wave convection, diffusion and dispersion in channels are represented in terms of variables characteristic of the channel and the flow. These processes are the result of contributions of terms in the momentum equation, and when expressed in nondimensional form, their relative magnitudes indicate appropriate simplifications of this equation. For example, the magnitude of the dimensionless physical diffusion coefficient of open channel flow waves is helpful when considering the justification for basing an analysis upon the diffusion-free kinematic wave theory. In general, relatively short-period waves in rivers are significantly affected by diffusion. The analysis also indicates that inertia has a small effect upon flow waves in natural channels at relatively small Froude numbers. This

conclusion is supported by the analyses of Ponce et al. (1978) and Henderson (1963) for flow in tailwaters, but contradicts the general belief that inertia is important in rapidly varying flows.

The analyses provided physical insights that guided our model selection. The inertia-free diffusion wave flow routing model of Koussis (1976) was chosen, and modifications were made as necessary for application to tailwater flow. The continuity equation that forms the basis of the model is a quasi-linear hyperbolic equation for discharge as a function of position and time. Exact solutions of this equation do not exhibit the diffusion necessary to simulate wave movement in most natural rivers. Through analysis of the numerical solution, however, it is possible to quantify numerical diffusion and dispersion. The capability of the model is enhanced when the numerical diffusion and dispersion error terms are equated with the terms for physical diffusion and dispersion of flow waves developed from the dynamic equations.

The analysis of a numerical model, a basic step in model development, is frequently limited to the development of criteria that ensure a stable solution. Numerical models must be stable if the solution obtained is to be meaningful. Numerical stability requires that errors introduced in the solution do not increase in magnitude as the computation progresses. The conditions required for stability of a numerical scheme are frequently known, and numerical instability is generally apparent. The von Neumann and Hirt analyses have been used to develop stability conditions for many numerical models (Roache 1976).

Numerical solutions of the unsteady open channel flow equations, however, typically exhibit errors in both amplitude and phase that may not be apparent without further analysis. Numerical dissipation or diffusion causes the Fourier components of the solution and the errors to be damped. Numerical dispersion results when the wave celerity of each wavelength component differs. These differences in celerity tend to modify the wave form as the computation proceeds. The effects of numerical dissipation and dispersion upon the accuracy of the solution are subtle and difficult to interpret. An improved understanding of the dissipative and dispersive behavior of the numerical model enables the analyst to minimize, neglect or exploit these effects to enhance model accuracy and to better interpret computed results. In our case, numerical diffusion must be quantified and controlled to permit a model without physical diffusion to properly simulate flow that may be significantly affected by diffusion.

Though only strictly applicable to linear equations, the "modified equation" (Warming and Hyatt 1974) and von Neumann analyses are used to quantify the dissipative and dispersive behavior of the model in terms of parameters of the numerical solution. The analyses are complementary, each having particular strengths. The Hirt analysis is also used, and its model behavior predictions are compared with those of the other methods. A set of linear routings is used to demonstrate the predicted behavior of the model and to verify the adequacy of the expression for numerical diffusion developed in the modified equation analysis.

Finally, we demonstrate the benefits of careful model development and analysis by comparing diffusion wave model simulations with extensive field data from the Apalachia and Norris Dam tailwaters. These tailwaters have very different bed slope and roughness characteristics, spanning those of a large number of rivers of practical interest. The accuracy achieved with the model in these field applications verifies its generality for this problem class, and reinforces the utility of both the nondimensional statement of the dynamic equations and the linear analyses of numerical solution behavior.

PHYSICAL DIFFUSION AND DISPERSION IN OPEN CHANNEL FLOW

The development of a mathematical statement describing the important physical processes of a problem relies upon a clear physical understanding. In this section we will develop a framework for obtaining physical insights from the one-dimensional dynamic equations of flow in open channels.

Flow in unstratified or weakly stratified reservoirs and in rivers having a significant base flow is generally modeled using the dynamic equations. Standard numerical solutions of these equations fail, however, if the flow depth approaches zero. This condition is common in tailwaters of dams used to generate peak power, motivating the search for an alternate mathematical statement.

The dynamic equations of flow in open channels (St. Venant equations) are the most complete statements of the laws of conservation of mass and momentum is common use when the longitudinal direction is the important spatial dimension. The dynamic equations for a free-flowing river with a wide prismatic rectangular channel and no local inflow are

$$\frac{\partial y}{\partial t} + \frac{1}{B}\frac{\partial Q}{\partial x} = 0 \tag{1}$$

$$\frac{1}{g}\frac{\partial Q}{\partial t} + \frac{2Q}{gBy}\frac{\partial Q}{\partial x} + \left(By - \frac{Q^2}{gBy^2}\right)\frac{\partial y}{\partial x} - BvS_0 + \frac{1}{C^2B}\left(\frac{Q}{y}\right)^2 = 0 \tag{2}$$

where t = time
x = distance along the length of the channel
y = flow depth
Q = discharge
B = channel width
g = acceleration due to gravity
S_0 = slope of the channel bottom
C = Chezy conveyance coefficient.

If the coefficients of eq 1 and 2 are assumed constant at appropriate reference values, the equations can be combined and expressed in terms of a single dependent variable yielding

$$\frac{\partial Q}{\partial t} + \left[\frac{3Q}{2By}\right]\frac{\partial Q}{\partial x} + \left[\frac{Q^3 - gB^2y^3Q}{2gB^3y^3S_0}\right]\frac{\partial^2 Q}{\partial x^2} + \left[\frac{Q^2}{gB^2y^2S_0}\right]\frac{\partial^2 Q}{\partial x\,\partial t} + \left[\frac{Q}{2gBy^2S_0}\right]\frac{\partial^2 Q}{\partial t^2} = 0 \tag{3}$$

a hyperbolic equation. Equation 3 can be manipulated further to eliminate the second-order mixed and temporal derivatives giving

$$\frac{\partial Q}{\partial t} + c\frac{\partial Q}{\partial x} = D\frac{\partial^2 Q}{\partial x^2} + E\frac{\partial^3 Q}{\partial x^3} + \text{(Higher Order Terms)}$$

$$c = \frac{3Q}{2By} = \frac{dQ}{dA}$$

$$D = \frac{Q}{2BS_0}(1 - F^2/4)$$

$$E = \frac{Q^2}{2gB^2y^2S_0}\,D = F^2\,\frac{v}{2S_0}\,D \tag{4}$$

where c is wave celerity, A the channel cross-sectional area and F the Froude number, $v/\sqrt{gy}$. Kinematic and zero-inertia equations can be developed as simplified versions of the dynamic equations. If second and higher order terms in eq 4 are neglected, the approximation is termed kinematic and is free of physically based diffusion. When third and higher order terms are neglected, eq 4 contains positive physical diffusion and is a form of the zero-inertia model. Tracing through

the development of eq 4 reveals that the source of the diffusion term is primarily the water surface slope term of the momentum equation (eq 2). The dependence of D upon the Froude number results from including the inertia terms in the development. The physical dispersion coefficient E given in eq 4 is also positive. Its magnitude varies linearly with the magnitude of the diffusion coefficient, and quadratically with the Froude number. The existence of the dispersion term and the higher order terms follow from the inertia terms.

Equation 4 combines the opposing tendencies of wave diffusion and steepening due to nonlinear convection. Whitham (1974) showed that discontinuities in the flow (shock waves) are not possible if positive diffusion is present. A physical justification is needed for the application of kinematic wave theory, in which diffusion is neglected, or for a more complete description of the flow. With reference discharge Q_0 and spatial and temporal increments Δx and Δt, eq 4 is rewritten in dimensionless form in terms of $Q^* = Q/Q_0$, $x^* = x/\Delta x$, and $t^* = t/\Delta t$ as

$$\frac{\partial Q^*}{\partial t^*} + C_r \frac{\partial Q^*}{\partial x^*} = D^* C_r \frac{\partial^2 Q^*}{\partial x^{*2}} + E^* D^* C_r \frac{\partial^3 Q^*}{\partial x^{*3}} + \text{(Higher Order Terms)}$$

$$C_r = \frac{c\Delta t}{\Delta x}$$

$$D^* = \frac{D}{c\Delta x}$$

$$E^* = \frac{Q^2}{2gB^2y^2S_0\Delta x} = F^2\left(\frac{y}{2S_0\Delta x}\right) \qquad (5)$$

where C_r is the Courant number, D^* a dimensionless diffusion coefficient, and E^* a dimensionless dispersion coefficient. The magnitude of Δx is a characteristic of the wavelength. The value selected should provide adequate resolution of the features of all flow waves of interest. Magnitudes of Δt and Q_0 are not as critical as they appear in the same way in each term of eq 5.

The magnitude of D^* relative to 1 is a measure of the importance of diffusion relative to convection. When this quantity is significantly less than 1, convection is dominant over diffusion. Smooth, steep channels are therefore good candidates for shock formation and successful application of kinematic wave theory. Other analyses addressing the use of the kinematic wave approximation are given in Menéndez and Norscini (1982) and Ponce et al. (1978). The magnitude of E^* relative to 1 measures the importance of dispersion relative to diffusion. As E^* is proportional to the square of the Froude number, its magnitude is generally much less than 1. Consequently, wave dispersion in rivers is usually negligible.

In natural rivers, flow generally occurs at small Froude numbers. When the Froude number is significantly less than 1, eq 5 simplifies to a nondimensional convective diffusion equation. Cunge (1969) developed an equivalent dimensional equation by initially neglecting inertia. In the form of eq 5, the dynamic equations indicate that river flow is independent of inertia in many instances.

MODELING APPROACH

The analysis of the previous section indicates that an inertia-free simplification of the dynamic equations frequently contains all important physical processes. Flood routing in rivers and several other unsteady open channel flow problems have been adequately treated using simplified zero-inertia or kinematic wave models. Still, Cunge et al. (1980) state that routing methods based upon simplified equations may not be applicable in situations like flow in tailwaters where rapid stage and discharge variations occur.

The question of the validity of using simplified routing methods for rapidly varying tailwater flow can be investigated within the framework provided by the analyses of Ponce and Simons (1977), Ponce et al. (1978) and Henderson (1963). The linear analysis of Ponce et al. provides insight into attenuation and propagation characteristics of the simplified models relative to those of the full dynamic model. For a range of channel and flow parameters characteristic of tailwaters, attenuation and propagation errors resulting from neglecting inertia appear small.

Henderson (1963) compared terms of the momentum equation in an order-of-magnitude analysis for a wide rectangular channel. The acceleration terms were of the same order of magnitude and were related to the water surface slope term as

$$\frac{\text{acceleration term}}{\partial y/\partial x} = 0\,(F^2)\,. \tag{6}$$

As the Froude number of the flow in natural rivers is typically much less than 1, the acceleration terms are small relative to the water surface slope term. Henderson also compared the water surface and bottom slope terms, obtaining

$$\frac{\partial y/\partial x}{S_0} \propto \frac{\partial q/\partial t}{q^{2/3} S_0^{5/3}}$$

where q is the discharge per unit width. For flood flows in natural streams the magnitude of the water surface slope term is often small relative to the bottom slope term. In tailwaters, where sudden large-magnitude flow changes occur, $\partial q/\partial t$ can be large, and the water surface slope term can be expected to make an important contribution to the momentum balance. The importance of the water surface slope term is further enhanced if the river being modeled has a small bottom slope.

The analyses support the use of an inertia-free model for tailwater flow routing. Our analysis and that of Ponce et al. (1978) indicate the importance of diffusion, and the Henderson analysis yields the related result that water surface slope is an important part of the momentum balance. The zero-inertia model satisfies these requirements. The local and convective acceleration terms of the full momentum equation are neglected in this model. The abbreviated set of equations includes the water surface slope term which permits wave attenuation or diffusion, and can be solved without difficulty as the flow depth becomes small. Commonly in tailwaters, however, the water surface slope changes abruptly with the passage of the toe of a wave front, and a number of fronts may exist simultaneously. As a result, the complications of accurately locating each front and evaluating the water surface slope in the vicinity of a front must be introduced into the model.

The kinematic wave approximation is obtained by neglecting the water surface slope term in addition to the acceleration terms of the momentum equation. This additional simplification does not permit wave attenuation and can be a serious limitation if the river being modeled is long or mildly sloped. Numerical solutions of the kinematic wave equation, however, frequently exhibit wave attenuation resulting from the solution technique (Cunge 1969, Smith 1980). This numerical diffusion can be used to mimic the physical diffusion occurring in the channel and overcome the inherent model limitation to diffusion-free flows.

Simple model formulation makes application of a kinematic wave based routing technique to flow in tailwater streams attractive. Models based upon the kinematic wave approximation, including the well-known Muskingum model, determine flow at a point independent of downstream influences. These models do not require a downstream boundary condition and cannot account for the influence of downstream controls upon the flow. The ability of this group of models to correctly represent flow in rivers with long pooled reaches is therefore suspect. Smith (1980) found that a variable weighting factor in the numerical scheme, corresponding to a variable diffusion coefficient, allowed successful application of kinematic wave based models to flood routing

through flat, ponded reaches. He did not, however, resolve the importance of backwater effects upon rapidly varying flows found in tailwaters.

In conclusion, the tailwater flow model formulation should include variable wave attenuation and the contribution of the water surface slope to the momentum balance. As a physically meaningful downstream boundary is not generally available in tailwaters, models not requiring a downstream boundary condition are most readily applied. The diffusion wave model that is described, analyzed and tested in this report satisfies these requirements. The model is an adaptation for tailwaters (Ferrick 1980) of the flood routing model of Koussis (1976). Weinmann and Laurenson (1979) related this formulation to other simplified routing methods.

DESCRIPTION OF THE DIFFUSION WAVE FLOW ROUTING MODEL

The diffusion wave model for flow in tailwaters is a kinematic wave based approach that differs from most simplified routing methods in that both stage and discharge are computed at each point in the numerical grid. The conservation of mass equation is solved numerically for discharge. Exact solutions of the continuity equation deform but do not damp with time, so that diffusion, which is necessary for representation of important physical processes in tailwater flows, is not present explicitly. The numerical solution of this equation, however, is adjusted in the model to require numerical diffusion to mimic physical diffusion. An equation for the stream rating curve, which includes the zero-inertia form of the momentum equation, models river stage. The inclusion of the water surface slope term in this relationship generates a looped rating curve and provides an improved estimate of wave celerity. The pair of equations are coupled through the wave celerity and must be solved simultaneously.

The conservation of mass equation for flow in open channels can be written as

$$\frac{\partial Q}{\partial x} + \frac{1}{c}\frac{\partial Q}{\partial t} = q_i \tag{7}$$

where

$$c = \frac{dQ}{dA} = \frac{dx}{dt}$$

Q = discharge,
q_i = local inflow per unit length of the channel
A = cross-sectional area of the channel
c = wave celerity

Equation 7, which forms the basis of the model, is a first-order hyperbolic equation. This type of equation is advantageous for modeling tailwater flow because a downstream boundary condition need not be specified. For this same reason, however, backwater effects upon the flow cannot be taken into account.

The "method of lines" approach is used to obtain a solution of eq 7. In this method the spatial derivative is approximated with a finite difference expression, but the dependent variable remains continuous in the time domain. The partial differential equation for conservation of mass is thereby reduced to an ordinary differential equation. With the approximations

$$\frac{\partial Q}{\partial x} \approx \frac{1}{\Delta x}\left[Q_{j+1}(t) - Q_j(t)\right] \tag{8}$$

$$\frac{\partial Q}{\partial t} \approx \theta \frac{\partial Q_j}{\partial t} + (1 - \theta) \frac{\partial Q_{j+1}}{\partial t} \tag{9}$$

in which j is an index corresponding to the spatial location $x = j\Delta x$, and θ is a parameter of the numerical solution, eq 7 is rewritten as

$$\dot{Q}_{j+1}(t) + a\, Q_{j+1}(t) = a\, Q_j(t) + a\Delta x\, q(t) - \frac{\theta}{(1-\theta)} \dot{Q}_j(t) \tag{10}$$

where

$$a = \frac{<\bar{c}>}{\Delta x(1-\theta)} .$$

$\dot{Q}$ is the derivative of discharge with respect to time, and $<\bar{c}>$ is an averaged celerity in space and time over the cell of the computational mesh where the equation is applied. Equation 10 is a linear first-order ordinary differential equation. Assuming, for a small time increment, that the variation of $Q_j(t)$ is linear, that the values of the coefficients can be estimated, and that the local inflow is constant, the solution of eq 10 is

$$Q_{j+1}^{m+1} = C_1\, Q_j^{m+1} + C_2\, Q_j^m + C_3\, Q_{j+1}^m + C_4 \tag{11}$$

where

$$C_1 = 1 - \alpha$$

$$C_2 = \alpha - \beta$$

$$C_3 = \beta = \exp\left(\frac{-C_r}{1-\theta}\right)$$

$$C_4 = q\,\Delta x\,(1-\beta)$$

$$\alpha = \frac{1-\beta}{C_r}$$

$$C_r = \frac{<\bar{c}>\Delta t}{\Delta x} .$$

The local Courant number of the numerical grid cell C_r expresses the ratio of physical to numerical wave celerity, and m is the temporal index of the computational grid, $t = m\Delta t$.

The variable physical diffusion of the flow is represented by tuning the numerical diffusion inherent in the model. An expression for the model parameter θ that results from enforcing the physical/numerical diffusion balance is

$$\theta = 1 + \frac{C_r}{\ln\left[\frac{1+\lambda-C_r}{1+\lambda+C_r}\right]}$$

$$\lambda = \frac{<\bar{Q}>}{BS_0 <\bar{c}>\Delta x} (1 - F^2/4) \tag{12}$$

where discharge and wave celerity are averaged over the numerical grid cell, and B is the width of the channel. A necessary condition for stability of the model is that either $\theta \leq 0.5$ or $\theta < 1.0$ and $C_r \geq 1.0$. Equation 12 and the stability criteria for the model will be developed subsequently.

For small values of the Froude and Courant numbers, eq 12 is equivalent to the expression developed by Cunge (1969) for the weighting factor in the Muskingum model:

$$\theta = \frac{1}{2}\left(1 - \frac{<\bar{Q}>}{BS_0<\bar{c}>\Delta x}\right) . \tag{13}$$

Neglecting the inertia of the flow and the momentum contribution of the local inflow, the zero-inertia conservation of momentum equation for prismatic channels is

$$\frac{\partial y}{\partial x} - S_0 + S_f = 0 \tag{14}$$

in which S_f is the slope of the energy grade line.

The zero-inertia momentum equation inserted into Manning's equation yields an expression for the stream rating curve,

$$V = \frac{C_m}{n} R^{2/3} \left(S_0 - \frac{\partial y}{\partial x}\right)^{1/2} \tag{15}$$

where R is the hydraulic radius, n the Mannings roughness coefficient, and C_m a constant that is dependent upon the system of units. To obtain a relationship that is consistent with the downstream-progressing discharge calculation (eq 11), the spatial derivative in eq 15 is replaced with a quantity determined at a point. If the energy slope is adequately large, arguments from kinematic wave theory can be used, and eq 15 can be rewritten in a form of the "Jones formula" as

$$V = \frac{C_m}{n} R^{2/3} \left(S_0 + \frac{1}{c^2 B} \frac{\partial Q}{\partial t}\right)^{1/2} . \tag{16}$$

With a finite difference approximation of the time derivative in eq 16 and the assumption of a wide rectangular channel, the flow depth is determined as

$$y = \left[\frac{Q n}{C_m B \left(S_0 + \frac{Q - Q_0}{c^2 B \Delta t}\right)^{1/2}}\right]^{3/5} . \tag{17}$$

The accuracy of the flow depth calculation using eq 17 depends upon the validity of the kinematic wave approximation. In response to decreasing flow in a river reach having a small bottom slope, the denominator of eq 17 may decrease more quickly than the numerator, causing the calculated stage to increase. This unphysical result signals the need for an alternate equation for the calculation of flow depth. If the definition of celerity is approximated as

$$c = \frac{dQ}{dA} \approx \frac{\Delta Q}{B \Delta y}$$

then an alternate equation for flow depth can be found:

$$y = y_0 + \frac{1}{cB} (Q - Q_0) . \tag{18}$$

The remaining unknown to be determined is wave celerity. As discussed by Henderson (1963), the celerity of a kinematic or zero-inertia flood wave is related to the flow velocity by a multiplier

that depends upon the channel shape and energy slope model used. The wave celerity of steep-fronted tailwater releases is also dependent upon the flow depth on either side of the wave front. In the extreme case of a rapid flow release to a previously dry channel, the celerity of the front must equal the velocity of the flow immediately behind it. The monoclinal rising wave is a translatory wave of stable form. If rising tailwater releases are presumed to be monoclinal waves during passage through a reach Δx, then an expression for wave celerity can be obtained. For a wide rectangular channel, with the Chezy equation used to describe the energy slope, the expression for wave celerity is

$$c_j = \left[\frac{1 - (y_{j+1}/y_j)^{3/2}}{1 - (y_{j+1}/y_j)}\right] V_j . \tag{19}$$

For slowly rising hydrographs, eq 19 yields the familiar result for celerity of a flood wave, $c = 1.5 V$. On the recession side of the hydrograph, the wave celerity used in the model is the value for flood waves.

The water surface slope is largely responsible for diffusion of flow waves and the existence of a looped rating curve in rivers. In the model, however, diffusion is generated numerically with the θ parameter and does not depend directly upon the water surface slope term. The depth corresponding to a given discharge varies depending upon the evaluation of the water surface slope (eq 17), and is lower during the rising limb of a hydrograph than during the falling portion of the hydrograph. This in turn affects the modeled discharge and wave celerity through eq 11 and 19, respectively.

To advance the routing one time step, eq 6 is solved at each grid point using values of Q and c computed at the previous time step to evaluate the coefficients. The values of flow depth and celerity are then updated with eq 17 through 19. The updated values are used to reevaluate the coefficients of eq 11, and the iteration repeats. A converged solution is reached when each of the flow values computed at successive iterations agrees within a set tolerance. In simulations performed at small Courant numbers a good initial estimate of the solution is available from the previous time step, and convergence is generally rapid.

The parameter θ varies locally with the flow and is continually updated during the iterative process. Values of the wave celerity and the corresponding Courant number vary along the channel. The model time step is determined from a limitation imposed upon the maximum Courant number. The Courant number limitation, required to preserve accuracy, has a numerical value that is dependent upon flow conditions.

ANALYSIS OF THE NUMERICAL MODEL

The development of a numerical model should include a thorough analysis of the solution technique. We will analyze the diffusion wave model with several linear techniques in this section of the report. The difference expression for the continuity equation used in our model was compared by Koussis (1980) with the Muskingum model, a more widely used method for routing flow in open channels. The difference representation of this equation is repeated here for the case of no local inflow,

$$Q_{j+1}^{n+1} = (1 - \alpha) Q_j^{n+1} + (\alpha - \beta) Q_j^n + \beta Q_{j+1}^n \tag{20}$$

$$\beta = \exp\left(\frac{-C_r}{1 - \theta}\right)$$

$$\alpha = \frac{1 - \beta}{C_r}$$

$$C_r = \frac{c \Delta t}{\Delta x}$$

where m and j are indices of the temporal and spatial location on the computational grid, respectively.

The diffusion wave model as applied by Weinmann and Laurenson (1979) and as described above is nonlinear with coefficients that are dependent upon the local flow conditions. The calculation for Q is explicit, progressing in the downstream direction from a known flow rate at the upstream boundary and given initial conditions. At each new time level the model iterates until the change in computed flow at each grid point is below a specified tolerance.

Modified equation and Hirt analyses of diffusion wave model

Stability, damping and dispersion characteristics of a difference approximation to a partial differential equation can be investigated with the modified equation analysis of Warming and Hyett and with the Hirt analysis. The two analyses follow the same basic steps with one important exception.

Neglecting roundoff error, the modified equation represents the actual partial differential equation solved when a numerical solution is obtained from a difference equation. To obtain the modified equation for the difference scheme of eq 20, each term is expanded in a Taylor series about Q_j^m. Upon simplification, the resulting equation is

$$\frac{\partial Q}{\partial t} + c\,\frac{\partial Q}{\partial x} + \frac{c\Delta x}{2}\,\frac{\partial^2 Q}{\partial x^2} + \frac{\Delta t}{2}\,\frac{\partial^2 Q}{\partial t^2} + \frac{c\Delta t}{(1-\beta)}\,\frac{\partial^2 Q}{\partial x \partial t} + \frac{c\Delta x^2}{6}\,\frac{\partial^3 Q}{\partial x^3} + \frac{\Delta x^2}{2\alpha}\,\frac{\partial^3 Q}{\partial x^2 \partial t}$$

$$+ \frac{\Delta x \Delta t}{2\alpha}\,\frac{\partial^3 Q}{\partial x \partial t^2} + \frac{\Delta t^2}{6}\,\frac{\partial^3 Q}{\partial t^3} + (\text{Higher Order Terms}) = 0 \qquad (21)$$

The modified equation has an infinite number of terms. Terms which appear in the modified equation but are missing from the original differential equation represent a type of truncation error.

Properties of a difference scheme can be found by examining a truncated version of the modified equation. The time derivatives higher than first order and the mixed derivatives are eliminated from eq 21 to obtain an equation that is amenable to physical interpretation. Even-order spatial derivatives in the recast equation correspond to dissipative effects and odd-order spatial derivatives reveal dispersive properties of the model. In the Hirt analysis, the governing differential equation is used to simplify eq 21. A solution of the original differential equation will not, in general, satisfy the difference equation. Therefore, in the modified equation approach, eq 21 itself is differentiated and used in the simplifying process. The coefficients are assumed to be constant in both analyses. Differences between the two procedures for the diffusion wave model analysis appear in the coefficients of third and higher order spatial derivatives.

Following the modified equation approach, eq 21 becomes

$$\frac{\partial Q}{\partial t} + c\,\frac{\partial Q}{\partial x} = D\,\frac{\partial^2 Q}{\partial x^2} + E\,\frac{\partial^3 Q}{\partial x^3} + (\text{Higher Order Terms}) \qquad (22)$$

$$D = \frac{c\Delta x}{2}\left(\frac{2C_r}{1-\beta} - 1 - C_r\right)$$

$$E = \frac{c\Delta x^2}{6}\left[3C_r\left(\frac{2}{1-\beta} - 1\right) - 1 - 2C_r^2\left(1 - \frac{3}{1-\beta} + \frac{3}{(1-\beta)^2}\right)\right] .$$

Following Hirt's analysis, the analogous expression for E is

$$E_H = \frac{c\Delta x^2}{6}\left[3C_r\left(\frac{1}{1-\beta}\right) - 1 - C_r^2\left(\frac{3}{1-\beta} - 1\right)\right] . \qquad (23)$$

If third and higher order terms are ignored, eq 22 is a linear convective diffusion equation. The Fourier components of the continuum solution of this equation are

$$Q_k \, e^{ik(x-ct)-Dk^2 t}$$

where k is the wave number (2π/wave length) of the component, $i = \sqrt{-1}$, and Q_k is the amplitude of the component of wave number, k. The modified equation of the diffusion wave model (eq 22) can be rewritten in the form

$$\frac{\partial Q}{\partial t} = \sum_{p=0}^{\infty} \mu(2p+1) \, \frac{\partial^{2p+1} Q}{\partial x^{2p+1}} + \sum_{p=1}^{\infty} \mu(2p) \, \frac{\partial^{2p} Q}{\partial x^{2p}} \, . \tag{24}$$

The form of the solution of eq 24 is

$$Q(x,t) \approx e^{(a+ib)t} \, e^{ikx} \tag{25}$$

where

$$a = \sum_{p=1}^{\infty} (-1)^p \, k^{2p} \, \mu(2p), \quad b = \sum_{p=0}^{\infty} (-1)^p \, k^{2p+1} \, \mu(2p+1) \, .$$

As waves of large wave number cannot be resolved on the numerical grid, waves having small wave numbers are of primary importance in the numerical solution. For these waves the exponent a of eq 25 can be approximated as

$$a \approx -k^2 D \tag{26}$$

where D is the diffusion coefficient defined in eq 22. A dimensionless numerical diffusion coefficient $D^* = D/(c\Delta x)$ of the diffusion wave model is given in Figure 1 as a function of the Courant number for various values of θ. A positive diffusion coefficient in the modified equation is necessary for positive damping in the model and a stable numerical solution. A stable solution is obtained if either $\theta < 0.5$ or $C_r > 1.0$ and $\theta < 1.0$. Stability does not impose a restriction upon the maximum value of the Courant number, which presents the possibility of using large time steps in the model. Numerical dissipation increases as θ decreases and as C_r increases. In the low Courant number range, < 0.5, damping does not vary greatly with the Courant number.

Components of all wave numbers of the continuum solution of the convective diffusion equation are advected at c. After an increment of time Δt the components have each undergone a phase angle change, Φ_c, of

$$\Phi_c = -ck\Delta t = -C_r (k\Delta x) = -C_r \gamma \, . \tag{27}$$

For the difference approximation, celerity is a function of wave number (eq 25). The phase angle change of the numerical solution in time Δt is

$$\Phi_N = b\Delta t = k \, \mu(1)\Delta t + \Delta t \sum_{p=1}^{\infty} (-1)^p \, k^{2p+1} \, \mu(2p+1) \, . \tag{28}$$

The ratio of the numerical to continuum phase shifts yields an expression for the relative propagation speed of each Fourier component per time increment

$$\Phi_r = \Phi_N/\Phi_c = 1 - \frac{1}{c} \sum_{p=1}^{\infty} (-1)^p \; k^{2p} \; \mu(2p+1) . \tag{29}$$

Values of Φ_r greater than 1 indicate that the numerical solution component of wave number k will have a celerity greater than that of the continuum solution. The converse is true for values of Φ_r less than 1. Since small wave numbers are of primary importance in the numerical solution, eq 29 can be approximated as

$$\Phi_r = 1 + \frac{k^2 \mu(3)}{c} + 0(\gamma^4) \approx 1 + \frac{\gamma^2}{6} \left[3C_r \left(\frac{2}{1-\beta} - 1 \right) - 1 - 2C_r^2 \left(1 - \frac{3}{1-\beta} + \frac{3}{(1-\beta)^2} \right) \right] . \tag{30}$$

Equation 30 is plotted as a function of the Courant number for selected values of θ in Figures 2-4 for wavelengths of 24 Δx, 12 Δx and 6 Δx, respectively. For these wavelengths, the phase angle of the numerical solution predominantly lags that of the continuum solution. The discrepancy is largest for the shorter wavelengths, smaller values of θ and larger values of the Courant number. For the shorter wavelengths and Courant numbers greater than 1, the phase angle of the numerical solution varies strongly with the Courant number. The numerical solution is most likely to exhibit leading phase angles for waves of short wavelength with θ approximately 0.5.

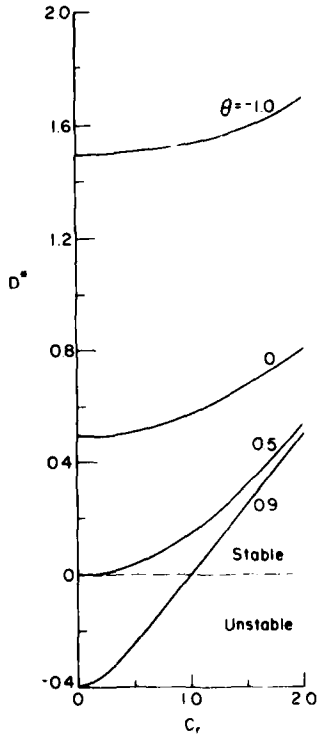

Figure 1. Dimensionless numerical diffusion as a function of Courant number for various values of the parameter θ. Values of D are based upon the modified equation analysis.*

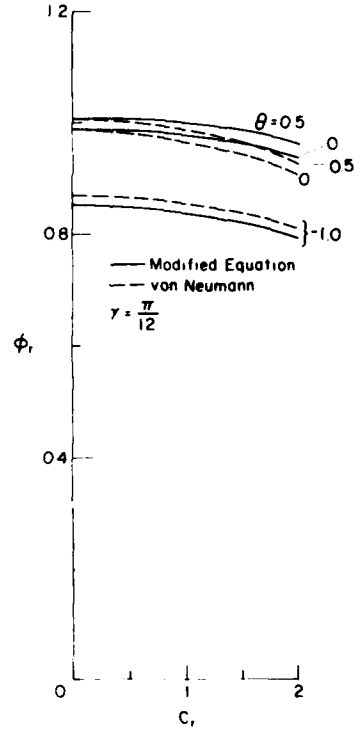

Figure 2. Ratio of numerical to continuum phase shifts in time Δt for 24-Δx wavelengths as a function of Courant number and various values of θ. One set of curves is based upon the modified equation analysis and one set upon the von Neumann analysis.

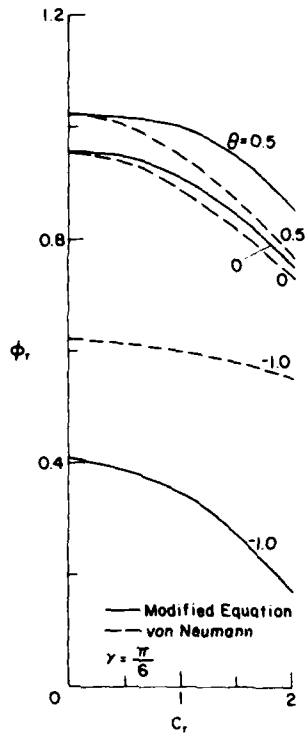

Figure 3. Ratio of numerical to continuum phase shifts in time Δt for 12-Δx wavelengths as a function of Courant number and various values of θ. One set of curves is based upon the modified equation analysis and one set upon the von Neumann analysis.

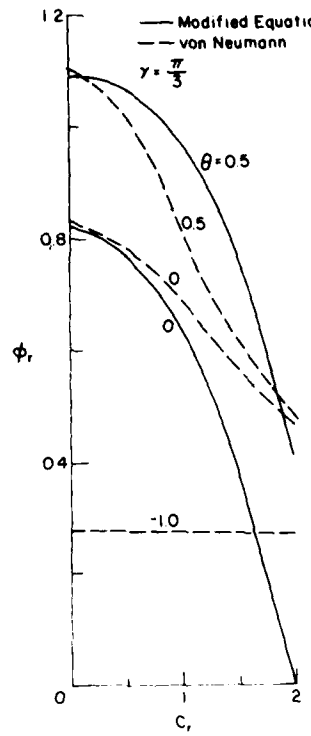

Figure 4. Ratio of numerical to continuum phase shifts in time Δt for 6-Δx wavelengths as a function of Courant number and various values of θ. One set of curves is based upon the modified equation analysis and one set upon the von Neumann analysis.

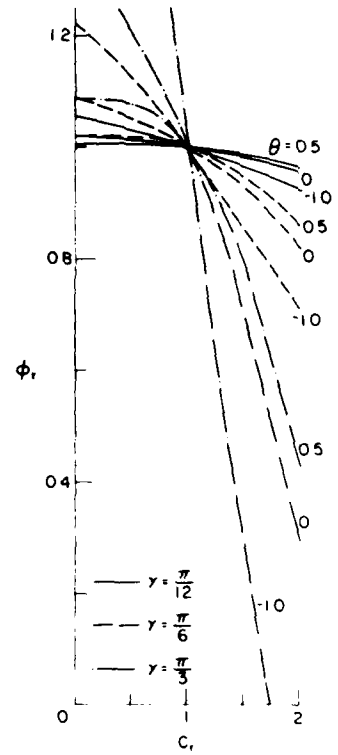

Figure 5. Ratio of numerical to continuum phase shifts in time Δt for 24-Δx, 12-Δx and 6-Δx wavelengths as a function of Courant number and various values of θ. The curves are based upon the Hirt analysis.

An analogous equation for the ratio of the numerical to continuum phase shifts based upon the Hirt analysis can be written by substitution of eq 23 for μ (3) of eq 30, yielding

$$\Phi_r \approx 1 + \frac{\gamma^2}{6}\left[3C_r\left(\frac{1}{1-\beta}\right) - 1 - C_r^2\left(\frac{3}{1-\beta} - 1\right)\right]. \qquad (31)$$

Equation 31 is plotted in Figure 5 as a function of the Courant number for the same wavelengths and θ values used with eq 30. This series of curves projects quite different dispersion behavior than the modified equation analysis. At a Courant number of 1, the Hirt analysis projects zero dispersion independent of wavelength and θ. Lagging phase angles are projected at higher Courant numbers, and all phase angles are leading at lower Courant numbers. Shorter wavelengths and lower values of θ are projected to have larger phase errors.

von Neumann analysis of the diffusion wave model

As a result of the truncation of terms in eq 26, the modified equation analysis does not provide information regarding the diffusive nature of the short wavelength Fourier components of the solution or of the error. These components are, at times, responsible for instability of a numerical solution. Similarly, the approximation in eq 30 limits the application of the modified-equation-based phase relationship to waves of relatively small wave number. In addition to its usual role of providing numerical stability criteria, the von Neumann analysis can be used to identify the relative damping and dispersion of Fourier components of all wave numbers.

The evolution of the numerical solution in a time step Δt is considered in this approach. The coefficients α and β of eq 20 are assumed to be constant. The solution of eq 20 can then be written as a Fourier series:

$$Q_j^n = \sum_k \tilde{Q}_k^n \, e^{ij\gamma} \tag{32}$$

where $\tilde{Q}_k^n$ is an amplitude function at time $n\Delta t$ of the Fourier component of wave number k. Each term of the difference equation is replaced by its k-th Fourier component. The spatial domain is assumed to be infinite, and boundary influences are not considered. The decay or amplification of each component is evaluated to investigate stability and damping of the numerical scheme by forming the ratio of the amplitude functions at two successive times, $n\Delta t$ and $(n+1)\Delta t$. Performing these operations upon eq 20 yields

$$r_k = \frac{\tilde{Q}_k^{n+1}}{\tilde{Q}_k^n} = \frac{\alpha + \beta\,(e^{i\gamma} - 1)}{\alpha + (e^{i\gamma} - 1)} \tag{33}$$

in which the complex number r_k is termed *the amplification factor. A necessary and sufficient* condition for stability of the solution is that the modulus of r_k be less than or equal to 1 for all integer values of k (Richtmyer 1957). An expression for the square of the modulus of r_k which follows from eq 33 is

$$|r_k|^2 = \frac{\alpha^4 + 2\alpha^2(\beta+1-\alpha)(\beta+1)(1-\cos\gamma) + 2\beta\,[2\beta(1-\alpha) + \alpha(\alpha-2)](1-\cos\gamma)^2 - 2\alpha^2\beta\sin^2\gamma}{\alpha^2 + 4\alpha^2(1-\alpha)(1-\cos\gamma) + 4(1-\alpha)^2(1-\cos\gamma)^2} \tag{34}$$

The square of the modulus of r_k must also remain less than or equal to 1 for all integer values of k for a stable numerical solution. When $|r_k|^2$ is equal to 1 for a component of wave number k, the numerical scheme is termed conservative or neutrally stable. Smaller values of $|r_k|^2$ correspond to larger inherent dissipation of the numerical scheme.

Long wavelengths are resolved over a large number of grid points. For these waves, γ is small and the following substitutions can be made in eq 34:

$$\sin^2\gamma \approx \gamma^2$$

$$1 - \cos\gamma \approx \gamma^2/2$$

$$(1-\cos\gamma)^2 \approx 0 \tag{35}$$

and eq 34 can then be simplified to yield

$$|r_k|^2 \approx \frac{\alpha^2 + [(1-\alpha) + \beta(\beta-\alpha)]\gamma^2}{\alpha^2 + 2(1-\alpha)\gamma^2} \quad . \tag{36}$$

The solution will be stable for long period waves if

$$\beta(\beta-\alpha) - (1-\alpha) < 0 \, . \tag{37}$$

This inequality is satisfied if either $\theta < 0.5$ or $C_r > 1.0$ and $\theta < 1.0$. These criteria are in agreement with those based upon the modified equation analysis. Figure 6 presents $|r_k|^2$ as a function of Courant number for two wavelengths ($24\Delta x$, $12\Delta x$) and selected values of θ (0.9, 0.5, 0.0, -1.0). Numerical damping is sensitive to C_r and θ, as was noted in the modified equation analysis, and exhibits the same trends. For long period waves having equivalent θ and C_r, the shorter wavelengths are more highly damped.

As mentioned above, the von Neumann approach permits analysis of short period waves. Assuming γ is equal to $\pi/2$, eq 34 becomes

$$|r_k|^2 = \frac{\alpha^2 - 2\alpha^3(1+\beta) + 2\alpha^2(1+\beta)^2 - 4\alpha\beta(1+\beta) + 4\beta^2}{\alpha^4 - 4\alpha^3 + 8\alpha^2 - 8\alpha + 4} \quad . \tag{38}$$

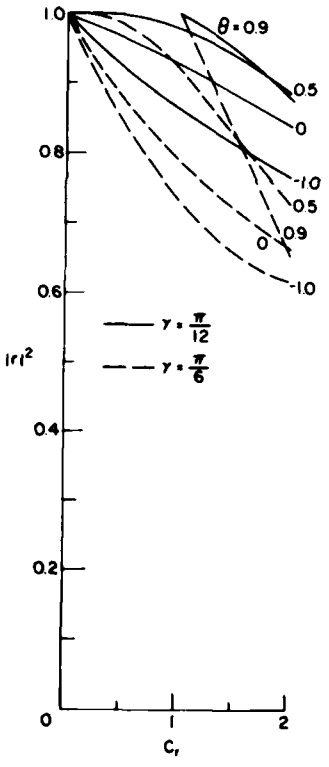

Figure 6. Square of the modulus of the amplification factor for 24-Δx and 12-Δx wavelengths as a function of Courant number and various values of θ.

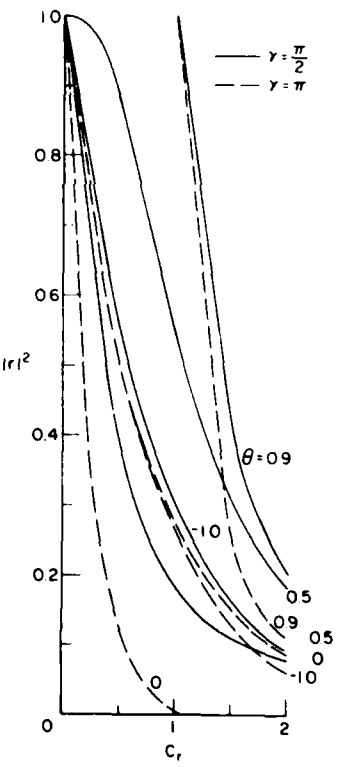

Figure 7. Square of the modulus of the amplification factor for 4-Δx and 2-Δx wavelengths as a function of Courant number and various values of θ.

Imposing the stability restriction on the square of the modulus of r_k requires that

$$\alpha^3 - \alpha^2 (\beta + 3) + 2 \alpha(\beta + 2) - 2 (\beta + 1) < 0 . \tag{39}$$

The stability limits developed for the long period waves also satisfy the requirement imposed by eq 39 for a short period wave. The $|r_k|^2$ is presented as a function of Courant number in Figure 7 for values of γ equal to both $\pi/2$ and π, the shortest wavelength resolvable on the numerical grid. Short period wave damping increases with Courant number and is a much stronger function of Courant number than for the long period waves. Also, damping generally increases as wavelength decreases. Wave propagation with a Courant number of 1.0 and θ of 0.9 is undamped for both short and long period waves. No limitation upon the minimum value of θ is necessary for stability of the model.

The dispersive properties of the numerical scheme can also be investigated using the von Neumann analysis. For small angles, the measure of an angle in radians is approximately equal to the sine of the angle. The phase angle of the numerical solution at time Δt is then

$$\Phi_N = \frac{\text{Imag}\,(r_k)}{|r_k|} . \tag{40}$$

For the diffusion wave model, eq 40 can be written as

$$|\Phi_N| = \sin\gamma \cdot C_r \left[\frac{1}{C_r^2 \sin^2\gamma + 1 + 2A + A^2}\right]^{1/2} \tag{41}$$

where

$$A = \frac{C_r (\beta^2 + 2\beta C_r - 1)(1 - \cos\gamma)}{(1 - \beta)^2} .$$

The ratio of the numerical to continuum phase angle is

$$\Phi_r = \frac{\sin\gamma}{\gamma} \left[\frac{1}{C_r^2 \sin^2\gamma + 1 + 2A + A^2}\right]^{1/2} . \tag{42}$$

Again, propagation in the numerical model matches that in the continuum solution of the convective diffusion equation if this ratio is 1 for a given wavelength. Equation 42 is plotted in Figures 2-4 for wavelengths of $24\Delta x$, $12\Delta x$ and $6\Delta x$ respectively. Though the values of Φ_r are not generally equal to those obtained using the modified equation analysis, all of the trends are in agreement. Unlike the modified equation approach, however, no restriction upon γ was used in the development of the equation for Φ_r. Therefore, for the shorter wavelengths (Fig. 4), the von Neumann analysis is likely to give a better estimate of the phase variation in the model. Numerical dispersion is typically the largest for short period waves or short period Fourier components of a wave. Equation 42 reveals that the shortest wave resolvable on the numerical grid is stationary.

LINEAR CASE STUDIES

A set of linear case studies is presented to demonstrate the utility of the modified equation and von Neumann analyses in representing model behavior. Figure 8 presents half sine waves, of wavelength $8\Delta x$ and $16\Delta x$, which will serve as initial conditions for the studies which follow. In each case, the wave celerity is held constant at 3 ft/s (0.91 m/s), independent of the flow. If in addition

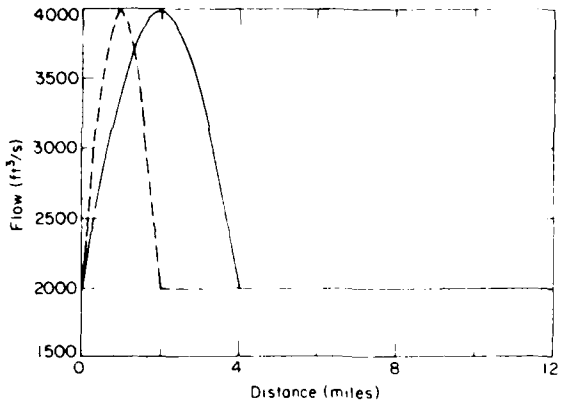

Figure 8. Half sine waves of wavelength 8- and 16-Δx that serve as initial conditions for the linear case studies.

to constant celerity, a constant diffusion coefficient is assumed, then the solution of the initial value problem posed by the linear convective diffusion equation and an initial condition of Figure 8 can be written as a Fourier series.

Initially, a key question will be addressed regarding the adequacy of the expression given by the modified equation analysis for the numerical diffusion inherent in the model. A 97-term Fourier series solution of the convective-diffusion equation with a diffusion coefficient calculated from eq 22 was obtained. This analytical solution is compared in Figure 9 with the corresponding numerical solution for each wavelength after the center of the wave has been advected 6 miles (9.7 km) downstream. Cases presented were projected in the analyses to have minimal dispersion and a range of diffusion. The damping evidenced in the numerical and analytical solutions are in agreement in all cases. The cases with θ equal to 0.9 and C_r of 1.0 exhibited essentially pure convection. No damping or phase error of any Fourier component of the solution was projected for this case by the von Neumann analysis. A small amount of dispersion, evidenced by a slight lag in the numerical solution, was present in the cases with θ of 0.0 and C_r of 0.1. This slight lagging phase error was projected by both the von Neumann and modified equation analyses (Figs. 2 and 3). By contrast, the Hirt analysis projected a leading phase error for these same cases (Fig. 5).

Several cases are presented to demonstrate the projected diffusive and dispersive behavior of the model. Figure 10 contains numerical and analytical solution comparisons for cases having a constant Courant number and selected values of θ, after the center of the wave has been advected 6 miles (9.7 km) downstream. The leading phase error of the longer wavelength components and the more extreme leading phase error of the short wavelength components are evident for the case in which θ is 0.5. This behavior was projected in Figures 3 and 4. Minimal damping of the short wavelength components (Fig. 7) is the other condition necessary for development of leading short period waves. A small amount of phase lag occurs as projected for the case with θ equal to 0.0. In this case, damping is large, especially of the short wavelength components. Larger damping and greater phase lag occur, as expected, when θ is set at -1.0. The Hirt analysis projects leading phase errors for all θ values when the Courant number is small. In addition, leading errors are projected to be more extreme at small values of $\theta (\leq 0.0)$.

For the cases presented in Figure 11, θ is held constant as Courant number is varied. As projected by the modified equation and von Neumann analyses, leading phase errors occur for Courant number 0.1, lagging phase errors occur for Courant number 4.0, and a minimal phase error is observed for Courant number 1.0. Numerical diffusion is again well represented by the expression developed using the modified equation approach.

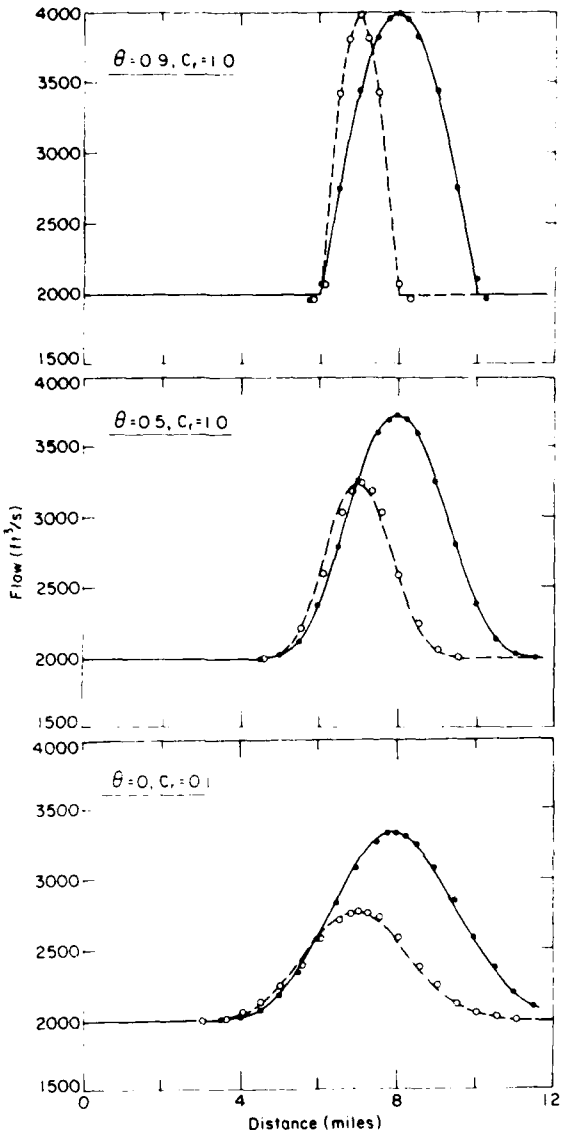

Figure 9. Comparison of numerical and Fourier series solutions for 8- and 16-Δx wavelengths after the center of the wave has propagated 6 miles (9.7 km) downstream. Cases shown were projected to have minimal dispersion and a range of diffusion by the modified equation and von Neumann analyses.

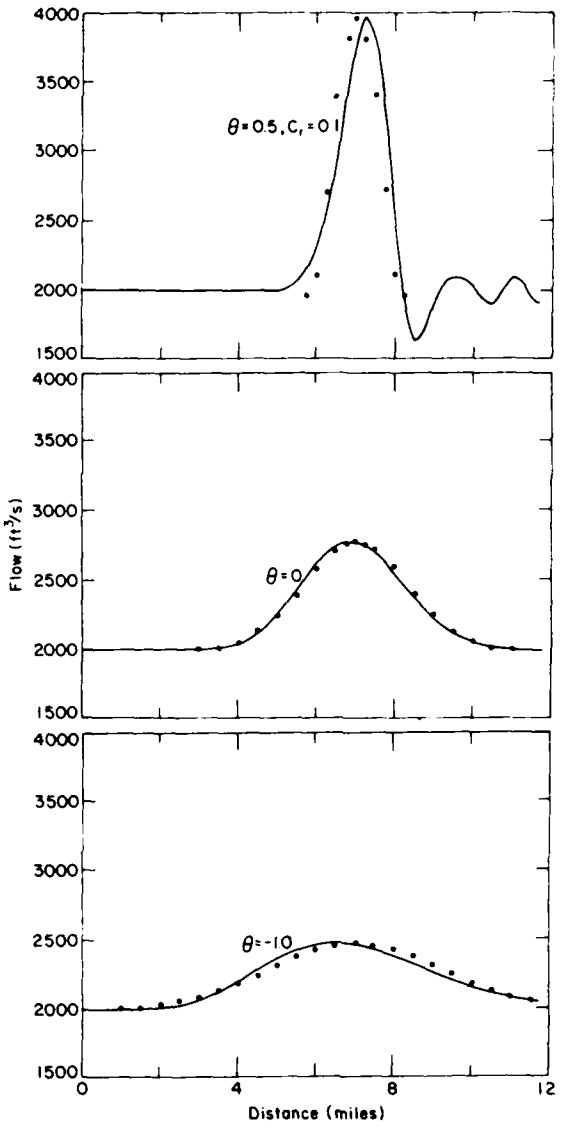

Figure 10. Comparison of numerical and Fourier series solutions for the 8-Δx wavelength and a fixed value of C_r = 0.1 after the center of the wave has propagated 6 miles (9.7 km) downstream.

In practice, cost considerations generally preclude the use of an extremely fine computational grid. An assessment of the adequacy of a given mesh relative to the flow features of interest in the prototype is an important part of model testing. The linear analyses have shown that numerical damping and phase errors increase with spatial grid size. To investigate these effects, the short period wave of Figure 8 was resolved on a coarse grid containing one-half the number of points used in Figure 8. Cases having parameters identical to those presented in Figure 10 were repeated using this coarse grid and are presented in Figure 12. As diffusion increases with the spatial mesh

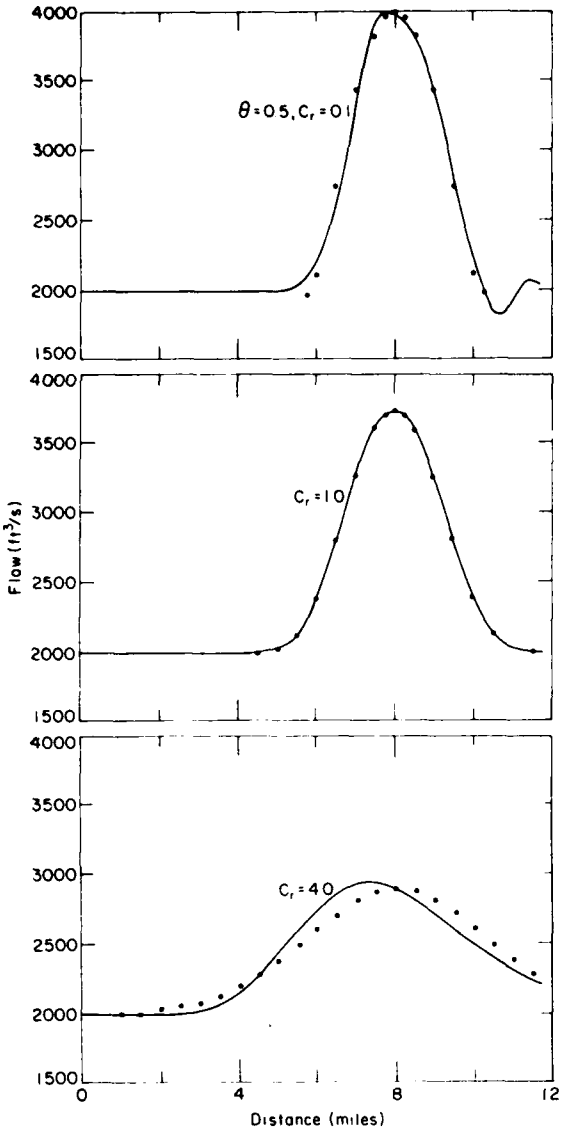

Figure 11. Comparison of numerical and Fourier series solutions for the 16-Δx wavelength and a fixed value of θ = 0.5 after the center of the wave has propagated 6 miles (9.7 km) downstream.

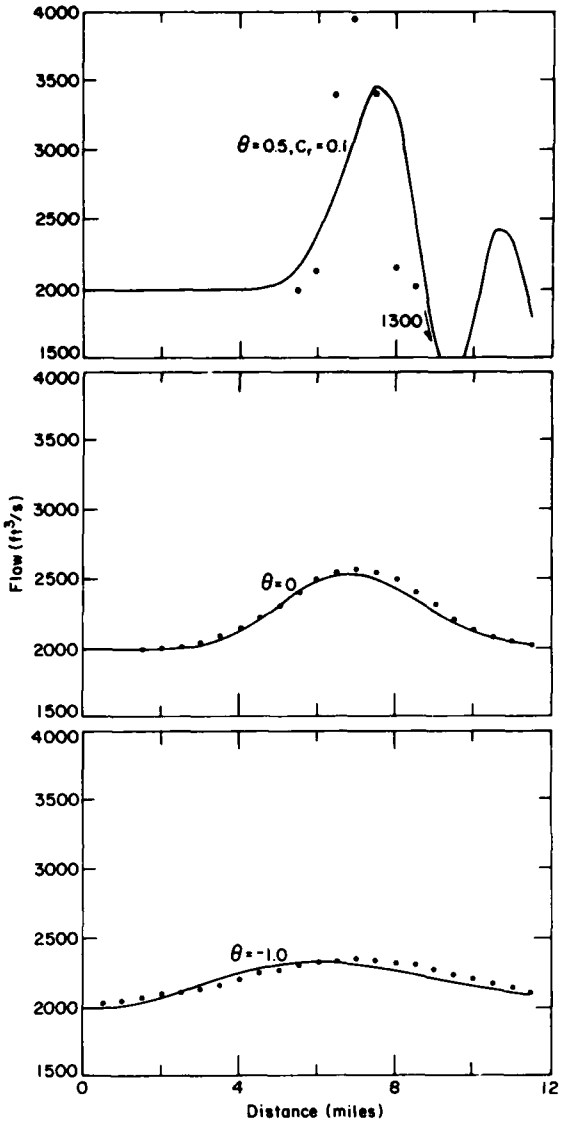

Figure 12. Comparison of numerical and Fourier series solutions for the shorter (8-Yx) wavelength resolved on a coarse grid after the center of the wave has propagated 6 miles (9.7 km) downstream. The wave had a 4-Δx initial wavelength relative to the coarse grid.

dimension Δx, damping is greater in the coarse mesh simulation for given values of θ and the Courant number. Large diffusion cases are well behaved; the wavelength of the flow quickly increases and numerical and analytical solutions correspond as before. The lightly damped case ($Cr = 0.1$, $\theta = 0.5$) largely retains its short wavelength and exhibits the same tendencies as its finer meshed counterpart. The peak flow, however, does not correspond to the analytical solution and the amplitude of the leading waves has increased. The wave period of interest is short enough, relative to the numerical grid, that a more accurate estimate of numerical diffusion is required. By

retaining more terms of the modified equation, a higher order estimate of diffusion could be made. It can be observed in Figure 10, however, that a refined mesh tends to correct the diffusion problem and yields decreased amplitudes of the leading waves. Adequate accuracy of the numerical solution on a coarse grid requires the presence of a large amount of diffusion. This requirement could preclude or impair the analysis of physically important cases.

ACCURACY CONSIDERATIONS OF THE NUMERICAL SOLUTION

The order of accuracy of the difference scheme is defined, in the modified equation analysis, as the power of the computational mesh dimension in the coefficient of the lowest order error term. If D of eq 22 is physically based, the numerical scheme is accurate to second order. Physically based values of D and E yield a third-order numerical solution.

Cunge (1969) and Smith (1980) equated coefficients of physical and numerical diffusion to enhance the capabilities of the Muskingum flow routing model. Koussis (1976) also followed this approach with the present diffusion wave model. In equating the diffusion coefficients, an error term in the numerical solution of the continuity equation is used to extend the physical basis of the model. An equation for the numerical weighting factor θ, in terms of Courant number and physical parameters of the flow and channel, is obtained by equating the diffusion coefficients of eq 4 and 22:

$$\theta = 1 + \frac{C_r}{\ln\left(\frac{1+\lambda-C_r}{1+\lambda+C_r}\right)} \tag{43}$$

where

$$\lambda = \frac{Q}{BS_0 c \Delta x}\ (1 - F^2/4)\ .$$

The value of θ is a function of position and time. For flow at relatively low Froude numbers common in rivers, eq 43 reduces to the equation given by Koussis. As evidenced in Figures 1, 6 and 7, model damping is dependent upon the Courant number and θ. As the Courant number approaches 1, the balance between physical and numerical diffusion is maintained by allowing θ to increase to compensate for increased damping as a result of the Courant number. As the Courant number is increased further, θ calculated from eq 43 may exceed the upper bound for model stability. In this instance, small values of diffusion cannot be attained in the model. If the diffusion balance is not enforced, the accuracy of the model will be degraded.

Strupczewski and Kundzewicz (1980) and Dooge et al. (1982) found in analyses of the Muskingum model that negative values of the weighting parameter are due to short model reach lengths. The same conclusion can be drawn from the value of θ expressed in eq 13 and 43. If negative values occur, θ can no longer be considered a weighting parameter. Instead, it is a parameter used to control or tune the diffusion of the numerical model.

In the interest of further enhancing the physical basis of the diffusion wave model, equating the coefficients of the physical and numerical dispersion terms of eq 4 and 22, respectively, would be desirable. This balance would provide improved model phase accuracy. However, the model does not contain a free variable in addition to the θ parameter with which to enforce balanced dispersion. Given θ of about 0.25 and $C_r < 0.5$, the dispersion term of the modified equation is approximately zero. Larger values of θ correspond to a positive numerical dispersion coefficient, and conversely, smaller θ values indicate a negative coefficient. The physical dispersion coefficient of eq 4 is always positive. To properly simulate physical dispersion requires that the shorter wavelength components propagate more quickly than the longer wavelength components. If the

dispersion coefficient in the model is negative, just the opposite will occur. Minimization of the imbalance is possible for many cases of interest with judicious selection of reach length. An adequate description of sharp-fronted waves of relatively short period that are encountered in tailwaters may, however, dictate fine resolution of computational mesh. Negative values of θ, which may then be required for proper diffusion in the model, will introduce some amount of lagging phase error in the simulation that will be most severe for the shorter wavelengths. Assessing the relative magnitudes of the dimensionless coefficients in eq 5 reveals that the magnitude of the dispersion term is small relative to that of the diffusion term. Therefore, imprecise modeling of dispersion is probably not a serious limitation. In any case, the insights obtained from these analyses remain valuable as the lagging phase error can be anticipated, improving the interpretation of model output.

FIELD STUDIES

Two extensive field tests were conducted to verify the diffusion wave model. One test was conducted in the Hiwassee River below Apalachia Dam and the other in the Clinch River below Norris Dam. Apalachia Dam is situated at Hiwassee River mile (HRM) 66 near the southern end of the Tennessee/North Carolina border. At the dam, the river has a drainage area of 1018 miles^2 (2636 km^2). In the 13-mile (20.9-km) study reach below the dam the river bed has a steep slope, dropping over 350 ft (106.7 m). The bed is extremely rough with large boulders and trees in the channel, creating roughness elements that are typically on the order of the flow depth. The pools located in the reach are relatively short. The bulk of the flow in this reach is normally diverted from the dam through a conduit to the Apalachia powerhouse located near the end of the reach. Therefore flow occurs only during floods and as a result of local inflows from a drainage area totaling 118 miles^2 (306 km^2).

Norris Dam is situated at Clinch River mile (CRM) 79.7 near Oak Ridge, Tennessee. The drainage area of the river at Norris Dam is 2912 miles^2 (7542 km^2). The physical characteristics of the Norris tailwater are significantly different from those of the Apalachia tailwater. The tailwater has a relatively mild bed slope, dropping about 25 ft (7.6 m) in the 13-mile (20.9-km) study reach immediately below the dam. Relative to that of the Apalachia Dam, a much greater percentage of the Norris tailwater is pooled at low flow. An individual pool located near the center of the study reach is over 2.5 miles (4.0 km) in length and has a bed slope of only 0.00012. In general, roughness elements on the Clinch River reach are much smaller than those on the Hiwassee River reach. In the pools, most of the roughness elements are submerged even during lengthy zero flow release periods from Norris Dam.

The physical characteristics of the Hiwassee River below Apalachia Dam and the Clinch River below Norris Dam span those of a large number of streams. Both rivers have typical alternating pool-riffle structures. The study reaches were located immediately below each dam where the features of the tailwater hydrograph are the sharpest and the effect of diffusion upon the flow releases is most pronounced. As the diffusion of a flow wave in a wide rectangular channel is inversely proportional to the bed slope (eq 4), much greater diffusion of the flow releases was expected in the Norris tailwater relative to that in the Apalachia tailwater.

Apalachia Dam tailwater

A field investigation of flow in the Apalachia Dam tailwater was conducted by personnel with the Tennessee Valley Authority (TVA) on 22-23 March 1979. The hydrograph during this study was produced with sluice gates at the dam and is given in Figure 13. River stage was recorded at HRM 62.8, 59.0, 56.9 and 53.0 during the test. The channel shape was approximated in the model as rectangular throughout the tailwater. Channel width and slope were obtained from USGS

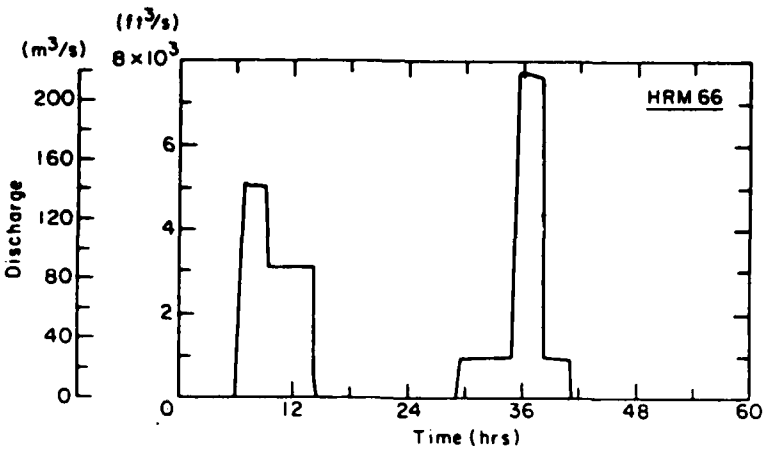

Figure 13. Apalachia Dam flow releases, 22-23 March 1979.

quadrangles. The tailwater channel width varied between 150 and 440 ft (46 and 134 m), averaging 280 ft (85 m), and the channel bed slope varied between 0.0027 and 0.0084. The Manning's roughness coefficient was estimated on the basis of field observations and was adjusted during model calibration. Calibrated roughness coefficients ranged between 0.04 and 0.07, averaging 0.066. Lateral inflow was initially neglected.

In addition to physical parameters characterizing the reach, model application requires a selection of numerical grid parameters. Both the linear analyses and past experience with model application provide guidance to initiate the selection process. We performed further studies of the laboratory test cases reported in Ferrick (1980) that have shown that mass balance and wave propagation speed errors in a model simulation are reduced with improved spatial grid refinement and by decreasing the maximum Courant number. Linear analysis of the model has revealed that damping and phase errors occur when the Δx chosen is large relative to wavelengths being routed. For these reasons, a spatial grid size of 5280 ft (1609 m) and a maximum Courant number of 1.0 were chosen for application of the model to the Apalachia tailwater. A limitation upon the minimum value of the parameter θ of 0.0 was imposed in the model to prevent lagging phase errors that occur with negative θ values.

A comparison of measured and computed stage is presented in Figure 14. The propagation of the 1000-ft^3/s (28.3-m^3/s) release in the model lags the data by a time that increases with distance downstream. The timing and magnitude of the other releases are accurately represented in the model. Due to the absence of the powerhouse discharge, the measured and computed stages are not in agreement at HRM 53. The diffusion of the waves during passage through the study reach is not large (Fig. 15), and the computed rating curves at the four stage measurement locations were not strongly looped. These observations indicate that the water surface slope term retained in the momentum balance may not be important. The water surface slope increases the effective channel slope at the wave front and causes an increase in the speed of wave propagation. The effect of neglecting this term upon the modeled flow was to lag the arrival of the rising limb of each hydrograph. Though the shape of the computed hydrograph was not significantly altered, discounting the water surface slope degraded the wave timing agreement between the model and the data.

A number of sensitivity studies were conducted in which the estimated input parameters, width and roughness, were varied in an effort to improve the agreement of the modeled and measured propagation of the 1000-ft^3/s (28.3-m^3/s) wave. Increased channel roughness caused a reduction in wave speed, an increase in steady-state stage for a given flow, and an extended duration of the

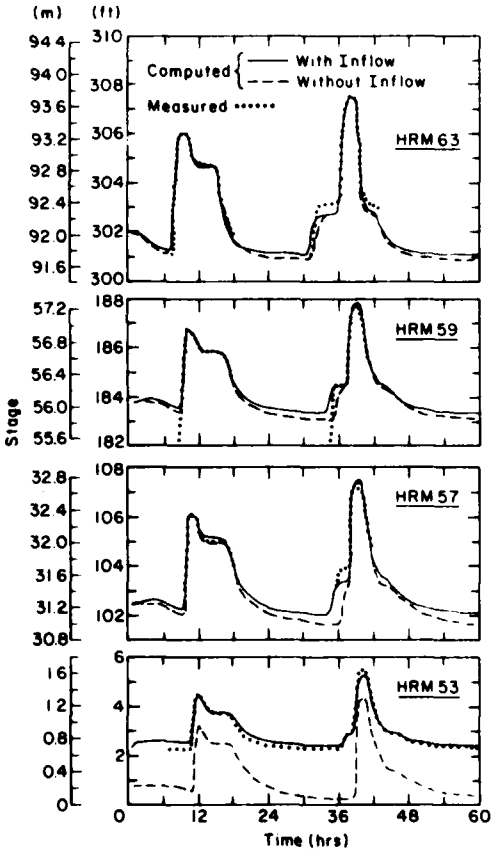

Figure 14. Measured and computed stage at several locations on the Apalachia tailwater. A maximum Courant number of 1.0, spatial grid resolution of 5280 ft (1609 m), and variable θ limited to positive values were conditions of the numerical simulation.

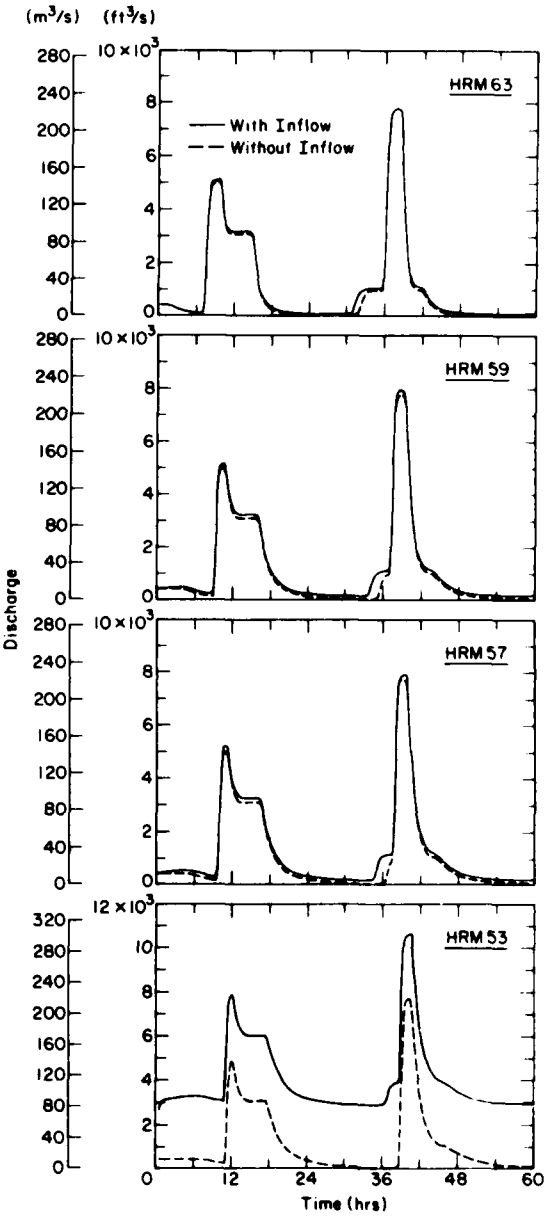

Figure 15. Computed discharge at several locations on the Apalachia tailwater. A maximum Courant number of 1.0, spatial grid resolution of 5280 ft (1609) m), and variable θ limited to positive values were conditions of the numerical simulation.

increased stage. Increased channel width caused a decrease in the magnitude of stage changes, a slowing of wave movement and a decreased period of increased flow. The overall agreement of model and prototype, however, was not improved.

A physically justifiable development that produced the correct propagation speed of the 1000-ft^3/s wave without significantly affecting the larger waves was the inclusion of local inflows. Local inflows, measured at 20 ft^3/s-mile (0.35 m^3/s-km) for the 3.5-mile (5.6-km) reach nearest the dam, were assumed to be representative for the tailwater. In addition, the known discharge at the powerhouse was included as a local inflow. Figure 14 presents a revised comparison between the model and prototype. At HRM 63 the only discrepancy concerns the stage increase during passage of the 1000-ft^3/s (28.3-m^3/s) flow. The effective channel width at low flow is less than at higher flow, but due to the assumption of a rectangular channel, measured stage at low flow is higher than the computed stage. At HRM 59 the averaged channel parameters of the model accurately describe the local channel characteristics except at times when only local inflows are present. Sensitivity studies indicated that the remaining discrepancies in the arrival times of the 1000-ft^3/s (28.3-m^3/s) wave at HRM 59 and 57 can be attributed to a lack of detailed inflow data. The river is pooled at low flow at mile 57, and as a result, the computed river stage at low flow at this location falls below the measured stage. Timing and magnitude of the larger flow arrivals are again accurately represented in the model. Further downstream, at HRM 53, model and prototype data agree closely, both in timing and magnitude for all the releases.

The flow releases in the Apalachia tailwater are lightly damped (Fig. 14-15), and experience with the model has revealed that this condition increases the tendency to compute an unphysical discharge value immediately preceding a sudden increase or decrease in discharge. This error was suppressed in the model by retaining the discharge computed at the previous time step. Numerical experiments were conducted to verify that this mechanism did not adversely affect the solution. Further experiments have shown that the tendency to compute an unphysical discharge is reduced by decreasing the maximum Courant number, or equivalently, the temporal grid resolution.

Dynamic waves of measurable size traveling ahead of the main flow and upstream wave movement resulting from wave reflections were not observed during the test. Together with these observations, the accurate simulation of wave propagation and damping of the rapidly varying flows generated for the Apalachia tailwater study confirm the negligible influence of the inertia terms for flow in steeply sloping tailwaters. The ability of the model to simulate flow in mildly sloping tailwaters, where the inertia terms are larger relative to other terms of the momentum balance, however, is more important practically and a more severe test case.

From the hydrographs presented in Figure 15 it is noted that the model accurately conserved mass. The limitation imposed upon the θ parameter, $\theta > 0.0$, permitted the numerical diffusion in the model to maintain the balance with the physical diffusion occurring in the stream and did not impair the accuracy of the simulation. The Manning's roughness model for the energy slope was adequate to characterize the effect of the large-scale roughness elements upon the flow. The physical justification for omission of backwater effects in the model cannot yet be judged. It is possible that the pooled reaches in the Apalachia tailwater were short enough to have a negligible effect upon the flow or that the addition of local inflow compensated for the effect.

Norris Dam tailwater

A 160-hour controlled release test (Fig. 16) was performed in the Norris Dam tailwater by personnel with the TVA on 1-7 July 1980, during which the variation of river stage was continuously recorded at CRM 78.85, 76.1, 73.6, 71.4, and 67.3. The long pool in the study reach was isolated by the placement of two of the recording gages at CRM 76.1 and 73.6. The channel shape was assumed in the model to be rectangular throughout the study reach. Prior to the test TVA personnel surveyed the tailwater for channel width and bed slope. Measured widths ranged between 260 and 540 ft (79 and 165 m), averaging 380 ft (116 m), and bed slopes varied between 0.00012

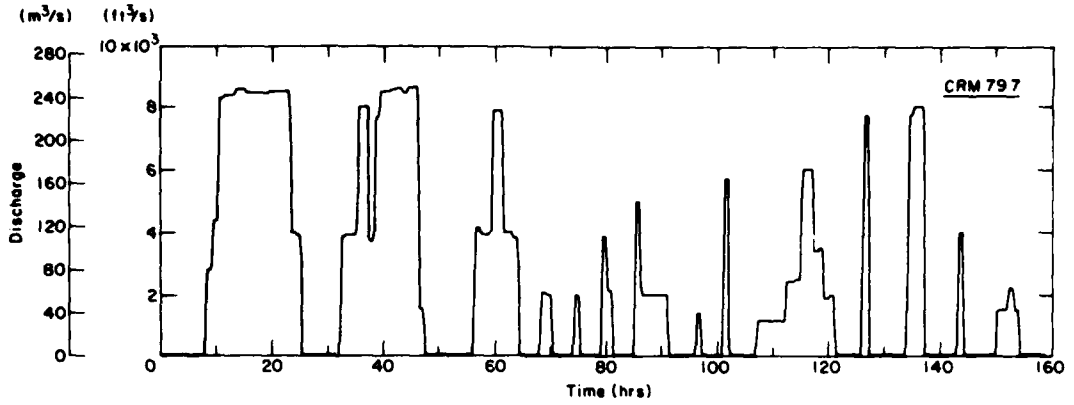

Figure 16. Norris Dam flow releases, 1-7 July 1980.

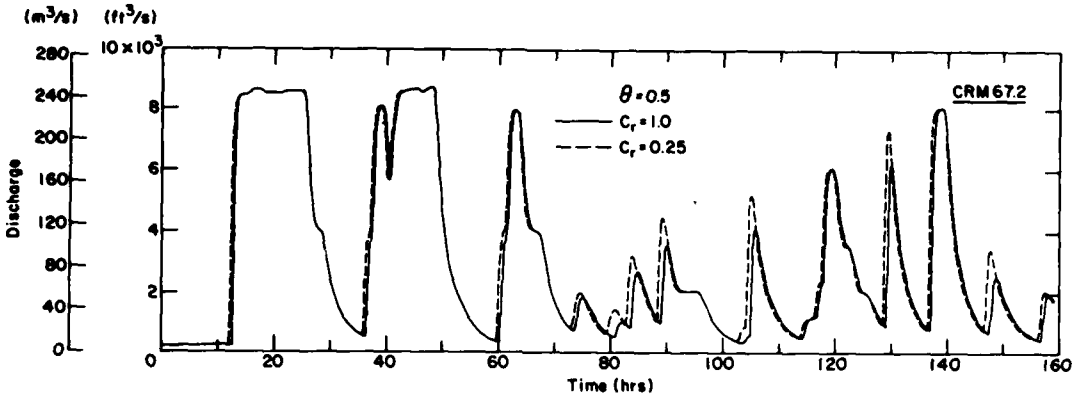

Figure 17. Hydrographs at downstream extent of Norris tailwater study reach computed with constant θ = 0.5, spatial grid resolution of 2640 ft (805 m), and maximum Courant numbers of 0.25 and 1.0.

and 0.00130. Local inflows were small during the test, averaging about 2 ft^3/s-mile (0.035 m^3/s-km), with point inflows of 19 ft^3 (0.54 m^3/s) from Coal Creek, the largest tributary, and 40 ft^3/s (1.13 m^3/s) of leakage past Norris Dam. Calibrated roughness coefficients that were used in the model simulations ranged between 0.015 and 0.035, averaging 0.026.

The Norris tailwater model required a relatively fine spatial resolution of 2640 ft (805 m) to provide stage and discharge information that was adequate to assess the effect of alternative flow release strategies upon the tailwater fishery, and to provide resolution necessary for accurate routing of short period releases. The linear analysis revelaed that the dissipative and dispersive characteristics of the model are sensitive to the Courant number and the θ parameter, in addition to the spatial grid resolution. To achieve optimal model accuracy, the limitations to be imposed upon the maximum value of the Courant number and the minimum value of the parameter θ were systematically addressed. Constant θ simulations for various values of the maximum Courant number and equal Courant number simulations with different minimum θ limitations were run to supplement the information supplied in the linear analysis.

Figure 17 presents computed flow at CRM 67.2 with a constant θ value of 0.5 and maximum Courant numbers of 0.25 and 1.0, respectively. The simulation at the higher Courant number exhibited greater model damping and lagging of the waves, relative to the lower Courant number

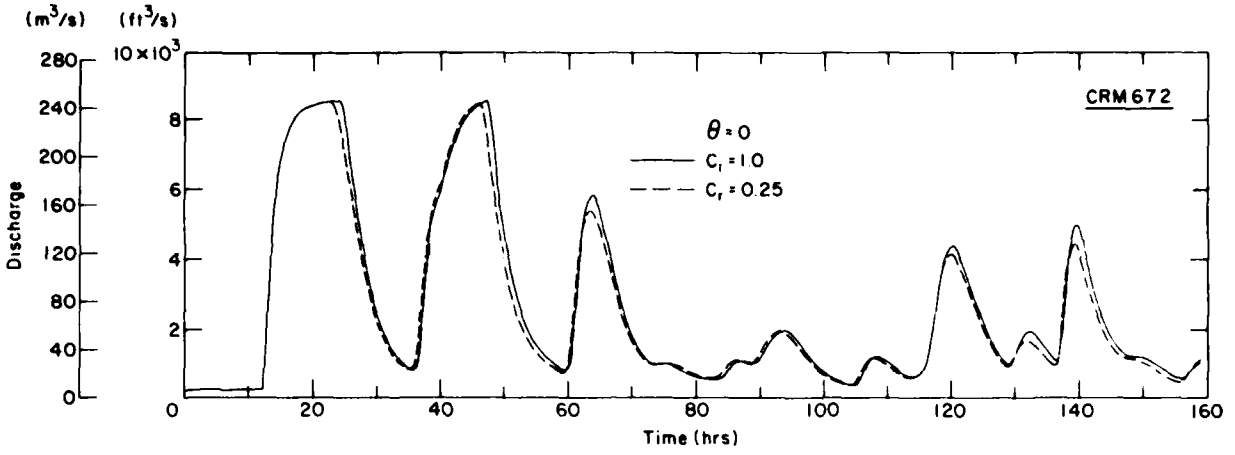

Figure 18. Hydrographs at downstream extent of Norris tailwater study reach computed with constant θ = 0.0, spatial grid resolution of 2640 ft (805 m), and maximum Courant numbers of 0.25 and 1.0.

simulation. This effect was especially pronounced for short period waves. Model damping in the small Courant number simulation was minimal. Based upon the linear model analysis, all of these tendencies were expected. Both simulations created mass, and the smaller Courant number case has a mass conservation error of 28% at CRM 67.2.

A comparison of the simulations with a constant θ value of 0.0, given in Figure 18, shows that wave propagation was slightly faster and wave attenuation was apparently greater for the simulation with a maximum Courant number of 0.25 than for the Courant number 1.0 simulation. The contradiction with the linear theory concerning wave attenuation is actually an effect of improved mass conservation which is seen as a quicker arrival of the tail of the wave. The bulk of the difference between the two simulations occurred in the long, nearly flat, pooled reach between CRM 76.2 and 73.7. Again, both simulations created mass, but the error was only 4% for the smaller Courant number case. Measured and computed stages with a constant θ value of 0.0 and a maximum Courant number of 0.25 agree reasonably well at all gages, although modeled damping is generally less than that in the prototype. This result indicates that a variable weighting factor is not essential for reasonably accurate modeling of flat, ponded river reaches.

Comparing the simulations of like Courant number in Figures 17 and 18 reveals model tendencies due to varying the θ parameter that were predicted in the linear analysis. The effect upon model damping of varying θ is much greater than the effect of varying the Courant number. For the cases in which θ is set at 0.0, the slopes of wave fronts are less steep, corresponding to increased diffusion relative to the cases where θ is 0.5. Also, the arrivals of the short wavelengths at CRM 67.2 are lagged in the θ equal 0.0 cases, relative to the θ equal 0.5 cases.

Further reduction of the Courant number did not affect the computed hydrograph for any of the constant θ runs at the downstream end of the study reach. Larger Courant number (> 2.0) simulations were attempted, but the iteration did not converge to a solution at the initial abrupt flow increase of the inflow hydrograph. This convergence problem was not resolved because of generally poor model accuracy at large Courant numbers.

The linear analysis of the numerical model indicated that negative values of θ, required to maintain the physical-numerical diffusion balance when fine numerical grids are used, introduce a small lagging phase error in the modeled results. Computed hydrographs for simulations having either a θ_{min} of 0.0 or no limitation upon θ_{min} are presented in Figure 19 for CRM 73.7 and 67.2. Figure 19 reveals that the timing of wave arrival is not greatly affected by the θ_{min} limitation, but wave damping and mass balance are extremely sensitive to the limitation. Limiting θ to

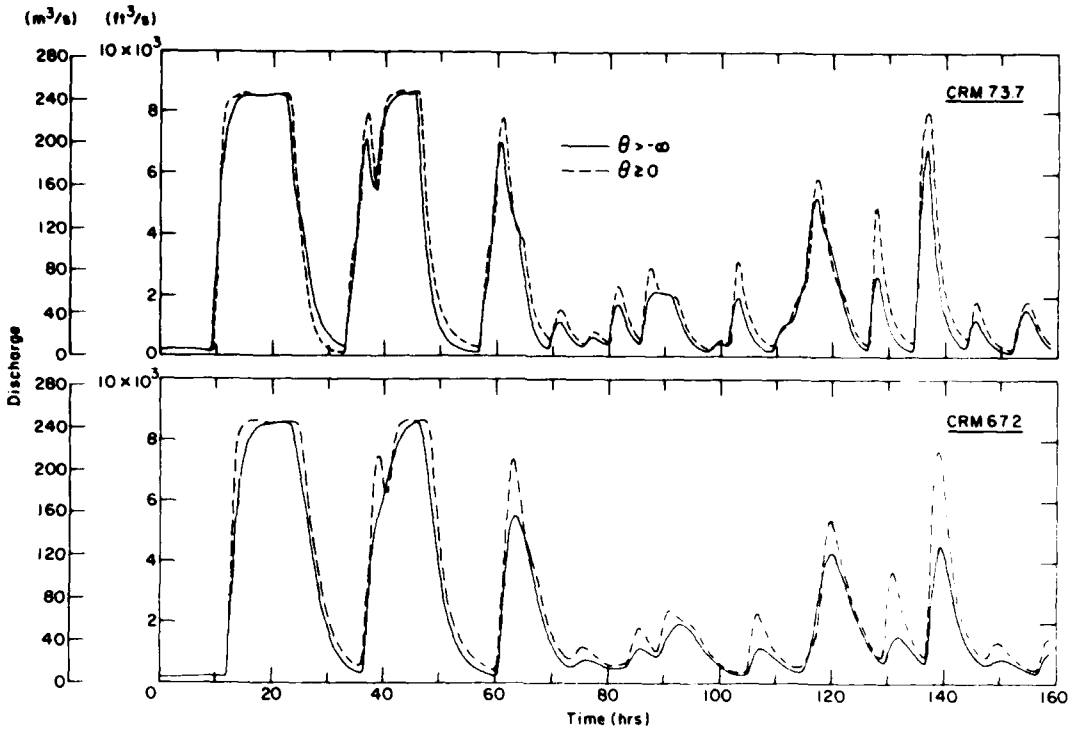

Figure 19. Hydrographs at downstream extent of the long pool and downstream extent of Norris tailwater study reach computed with maximum Courant number of 0.25, spatial grid resolution of 2640 ft (805 m), and variable θ either limited to positive values or allowing negative values.

positive values results in an increase in mass of 14% at the downstream end of the study reach. Relaxing the θ limitation to be greater than -1.0 reduces the increase of mass to 8%. Removing the limitation altogether yields a 4% decrease of mass at the downstream end of the reach.

Only minimal differences between the simulations existed upstream of the 2.5-mile (4.0-km) pooled reach where bed slope is relatively large and the θ_{min} limitation is imposed infrequently. Downstream of the pool at CRM 73.7, the flow and stage differences between the simulations are pronounced and continue to increase to the downstream extent of the study reach. Much larger wave diffusion is expected and is evident in the results of the simulation without a minimum θ limitation. Limiting θ to positive values did not produce attenuation of the modeled stages that was adequate to reproduce the prototype stage measurements.

A comparison of measured and computed stages without a θ_{min} limitation at five locations on the tailwater is given in Figure 20. The stage measurement locations do not coincide exactly with the modeled sections and proper interpretation of the offsets between measured and computed stage requires that these differences be considered. Overall agreement between the model and the data on wave timing, damping and shape is excellent. At the upstream-most gage (CRM 78.85) the model (CRM 78.7) reproduces the shape and timing of all the releases. An error in the chart speed of the stage recorder beginning at hour 100 leads to an increasing timing discrepancy toward the end of the test.

In Figure 20 the gage at the head of the long pool, CRM 76.1, is compared to the model output at CRM 76.2. The timing of the wave arrivals is well represented in the model. The modeled stages for the smaller waves are slightly less damped than in the prototype. In the pool, almost all roughness elements were submerged at low flow. Small, but physically reasonable, values of Manning's roughness, 0.015, were required to attain the proper depths of flow in the model for the pooled

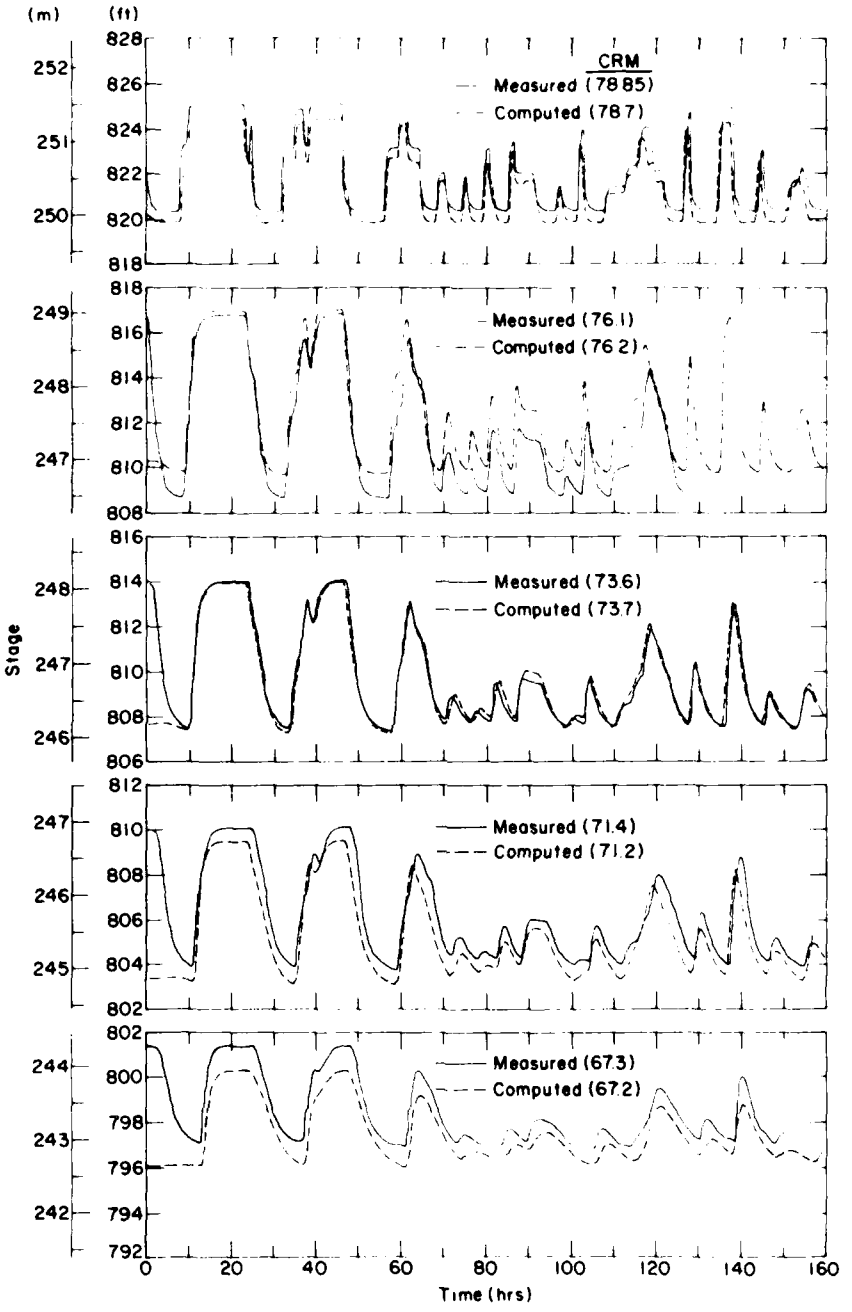

Figure 20. Measured and computed stage at several locations on the Norris tailwater. A maximum Courant number of 0.25, spatial grid resolution of 2640 ft (805 m), and variable θ without a lower bound were conditions of the numerical simulation.

reach. At the downstream end of the long pool, CRM 73.7, the wave shape and damping is well represented in the model. Only the smaller waves with short wavelengths are lagged in the model. The linear analysis of the model projected this behavior for short period waves through reaches where diffusion is large and the value of θ required for adequate diffusion in the model is small or negative.

Comparison between the stage data at CRM 71.4 and the numerical simulation at CRM 71.2 also reveals excellent model-prototype agreement. The origin of the timing error of the wave arriving at hour 136 is most likely cumulative, as this error is also evident in the model-prototype comparison at CRM 73.7. Finally, the comparison between prototype stage at CRM 67.3 and modeled stage at CRM 67.2 is again excellent. Due to negative θ values in the model, small, short period waves arriving between hours 70 and 90 lag slightly in the simulation.

The success of the simplified flow routing model of the Norris tailwater has important implications. The presence of backwater reaches in natural rivers does not significantly affect unsteady flow waves and need not be considered explicitly. Pooled reaches are adequately characterized by a small bottom slope and roughness. Again in this study, dynamic waves were not observed moving ahead of the main flow or propagating upstream as a result of a wave reflection. The reproduction of all features of the measured stage-time traces by the model demonstrates that steep-sided hydrographs in a mildly sloping stream are not affected significantly by inertia. As the relative importance of the inertia terms is greatest for these conditions, it follows that inertia is unimportant in shallow, free-flowing rivers. The extension of this conclusion to deeper rivers was indicated by Stoker (1957) in his study of rapidly rising flood waves on the Ohio River. He reported that the first measurable disturbance traveled far behind the initial dynamic wave at the wave speed used in simplified routing methods.

CONCLUSIONS

Physically based relationships for the diffusion and dispersion coefficients that describe wave movement in rivers were developed from a linear analysis of the dynamic equations of open channel flow. These relationships revealed that the magnitudes of the coefficients are related and that each is positive. By recasting the resulting equation in dimensionless form, insight regarding the relative magnitudes of the convection, diffusion and dispersion terms describing a river flow wave can be obtained. The magnitudes of these terms reflect upon the importance of the physical processes affecting the flow, and provide justification for using simplified models. For example, both the adequacy of the kinematic wave approximation and the potenital for shock formation in the channel are evaluated from the relative magnitude of the dimensionless diffusion coefficient. In general, diffusion of short-period waves is an important process that cannot be neglected.

The diffusion wave model for flow in tailwater streams is a simplified inertia-free routing model that allows variable wave diffusion and does not require a downstream boundary condition. The modified equation and von Neumann analyses provided stability, diffusive and dispersive characteristics of the model. The analyses are complementary, each having its particular strengths. Identical stability conditions, developed with each approach, revealed that stability does not impose a time step limitation upon the model.

The dissipative and dispersive characteristics of the model are sensitive to the selection of spatial grid resolution, the Courant number and the θ parameter. As revealed in the von Neumann analysis, model damping increases as wavelength relative to the spatial grid length, Δx, decreases. Both analyses showed that damping increases as θ decreases and as the Courant number increases. An expression quantifying the numerical diffusion of the model was an important result of the modified equation analysis. This expression was found to be an accurate representation of numerical damping. The von Neumann and modified equation analyses of model phase error concurred

and were supported over wide ranges of θ and the Courant number by the linear routing studies. The frequently utilized Hirt analysis yielded incorrect phase relationships. The routings and analyses revealed that damping and phase errors occur when the spatial grid is overly coarse relative to wavelengths of interest.

Guided by the linear analyses, selection of the spatial mesh dimension and the maximum Courant number can be made a priori to achieve optimal accuracy for a given application. The only calibration required for model application is the adjustment of Manning's roughness.

The capabilities and accuracy of the diffusion wave model are enhanced by allowing the parameter θ to vary so that a balance is maintained between physical and numerical diffusion. The numerical stability of the model does not place a lower bound on the value of θ. The limitation specified in many simplified models–that the weighting parameter applied to the time derivative, in this case θ, be greater than 0.0–should not be generally applied. Mildly sloping rivers, modeled with a fine spatial mesh for adequate wave resolution, require negative values of the weighting parameter for proper wave diffusion.

A physical/numerical dispersion balance eliminating model phase error cannot be maintained in the diffusion wave model simultaneously with the diffusion balance. Negative values of θ cause some amount of lagging phase error in the simulation that will be largest for the shorter wavelengths. The phase lag introduced in the Norris tailwater simulation as a result of allowing negative values of θ was minimal, noticeable only for small, short-period waves. Phase lag was not apparent in the Apalachia tailwater simulation where balanced diffusion was maintained with positive values of θ. For many cases of interest, phase error can be minimized by judicious selection of numerical parameters.

The release hydrographs and measured stage data from the Apalachia and Norris Dam tailwaters provided a discriminating test of model performance for wide ranges of bed channel slope and roughness. The effect upon the flow of numerous large-scale roughness elements in the Apalachia tailwater channel was adequately described by Manning's equation. The water surface slope term in the stage-discharge relationship was necessary even in this steeply sloping river to accurately model the propagation speed of the flow releases. Neglecting this term caused a time lag of each wave arrival. The inclusion of local inflow in the Apalachia model was needed to correctly propagate the small flow release. Correct wave celerity of this release could not be achieved through model calibration.

The ability of the model to simulate flow in both tailwaters demonstrates its generality for routing rapidly varying unsteady flow in rivers. As expected, the release hydrograph in the Apalachia tailwater experienced a small amount of diffusion relative to that in the Norris tailwater. In each case, the effect of diffusion upon the flow was reproduced with the diffusion wave model. Both tailwater studies indicated that backwater effects upon the flow of pooled river reaches need not be modeled explicitly.

The relative importance of the inertia terms in the momentum equation is greatest for steep-sided hydrographs in mildly sloped streams. In the Norris Dam tailwater test, however, dynamic waves of a measurable size propagating in either the upstream or downstream direction were not observed. These observations coupled with the success of the inertia-free Norris tailwater model support analytical findings that inertia is not significant in shallow, free-flowing rivers where flow typically occurs at relatively small Froude numbers.

LITERATURE CITED

Cunge, J.A. (1969) On the subject of a flood propagation computation method (Muskingum method). *Journal of Hydraulic Research*, 7(2): 205-230.

Cunge, J.A., F.M. Holly, Jr., and A. Verwey (1980) *Practical Aspects of Computational River Hydraulics*, Marshfield, Mass.: Pitman Publishing Inc., 420 pp.

Dooge, J.C.I., W.G. Strupczewski and J.J. Napiorkowski (1982) Hydrodynamic derivation of storage parameters of the Muskingum model. *Journal of Hydrology*, **54**: 371-387.

Ferrick, M.G. (1980) Flow routing in tailwater streams. In *Computer and Physical Modeling in Hydraulic Engineering* (G. Ashton, Ed.), ASCE, New York, pp. 192-208.

Henderson, F.M. (1963) Flood waves in prismatic channels. *Journal of the Hydraulics Division*, ASCE, **89**(HY4): 39-67.

Koussis, A.D. (1976) An approximative dynamic flood routing method. International Symposium on Unsteady Flow in Open Channels, University of Newcastle-upon-Tyne, England, 12-15 April, L1-1-L1-12.

Koussis, A.D. (1980) Comparison of Muskingum method difference schemes. *Journal of the Hydraulics Division*, ASCE, **106**(HY5): 925-929.

Menéndez, A.N. and R. Norscini (1982) Spectrum of shallow water waves: An analysis. *Journal of the Hydraulics Division*, ASCE, **108**(HY1): 75-94.

Ponce, V.M. and D.B. Simons (1977) Shallow wave propagation in open channel flow. *Journal of Hydraulics Division*, ASCE, **103**(HY12): 1461-1476.

Ponce, V.M., R.M. Li, and D.B. Simons (1978) Applicability of kinematic and diffusion models. *Journal of the Hydraulics Division*, ASCE, **104**(HY3): 353-360.

Richtmyer, R.D. (1957) *Difference Methods for Initial Value Problems.* New York: Interscience Publishers Inc., 238 pp.

Roache, P.J. (1976) *Computational Fluid Dynamics.* Albuquerque, N.M.: Hermosa Publishers, 446 pp.

Smith, A.A. (1980) A generalized approach to kinematic flood routing. *Journal of Hydrology*, **45**: 71-89.

Stoker, J.J. (1957) *Water Waves.* New York: Interscience Publishers Inc., 567 pp.

Strupczewski, W. and Z. Kundzewicz (1980) Muskingum method revisited. *Journal of Hydrology*, **48**: 327-342.

Warming, R.F. and B.J. Hyett (1974) The modified equation approach to the stability and accuracy analysis of finite-difference methods. *Journal of Computational Physics*, **14**: 159-179.

Weinmann, P.E. and E.M. Laurenson (1979) Approximate flood routing methods: A review. *Journal of the Hydraulics Division*, ASCE, **105**(HY12): 1521-1536.

Whitham, G.B. (1974) *Linear and Nonlinear Waves.* New York: Wiley-Interscience, 636 pp.

A facsimile catalog card in Library of Congress MARC format is reproduced below.

Ferrick, M.G.
Analysis of a diffusion wave flow routing model with application to flow in tailwaters / by M.G. Ferrick, J. Bilmes and S.E. Long. Hanover, N.H.: Cold Regions Research and Engineering Laboratory; Springfield, Va.: available from National Technical Information Service, 1983.
vi, 41 p., illus.; 28 cm. (CRREL Report 83-7.)
Prepared for Office of the Chief of Engineers by Corps of Engineers, U.S. Army Cold Regions Research and Engineering Laboratory under DA Project 4A161102 AT24,
Bibliography: p. 30.
1. Dams. 2. Flow routing. 3. Hydrology. 4. Mathematical analysis. 5. Numerical methods. 6. Peak power. 7. Rivers. 8. Water flow. 9. Waves

(see card 2)

Ferrick, M.G.
Analysis of a diffusion wave...
1983 (Card 2)

I. Bilmes, J. II. Long, S.E. III. United States. Army. Corps of Engineers. IV. Cold Regions Research and Engineering Laboratory, Hanover, N.H. V. Series: CRREL Report 83-7.

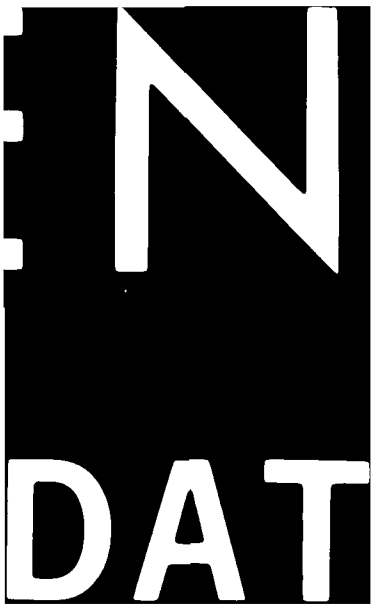
N
DAT